DEVELOPING A METHODOLOGY FOR CHARACTERIZING THE EFFECTS OF BUILDING MATERIALS' NATURAL RADIATION BACKGROUND ON A RADIATION PORTAL MONITORING SYSTEM

A Thesis

by

MATTHEW BLAKE FITZMAURICE

Submitted to the Office of Graduate Studies of
Texas A&M University
in partial fulfillment of the requirements for the degree of

MASTER OF SCIENCE

Approved by:

Chair of Committee,	Craig M. Marianno
Committee Members,	W. Dan Reece
	Sunil Khatri
Head of Department,	Yassin Hassan

December 2012

Major Subject: Nuclear Engineering

ABSTRACT

Trafficking of radioactive material, particularly special nuclear material (SNM), has long been a worldwide concern. To interdict this material the US government has installed radiation portal monitors (RPMs) around the globe. Building materials surrounding an RPM can greatly effect the detector's background radiation levels due to Naturally Occurring Radioactive Material (NORM). In some cases this effect is so great that the initial RPM setup had to be rebuilt.

This thesis develops a methodology for quick and efficient determination of the specific activity and composition of building materials surrounding a RPM to predict background levels, therefore determining the minimum detectable quantity (MDQ) of material. This methodology builds on previous work by Ryan et al by generating material and source cards for a detailed Monte Carlo N-Particle (MCNP) deck, based on an experimental RPM setup to predict the overall gamma background at a site.

Gamma spectra were acquired from samples of building materials and analyzed to determine the specific activity of the samples. A code was developed to estimate the elemental composition of building materials using the gamma transmission of the samples. These results were compared to previous Neutron Activation Analysis (NAA) on the same samples. It was determined that densitometry provided an elemental approximation within 5% of that found through NAA. Using the specific activity and material composition, an MCNP deck was used to predict the gamma background levels

in the detectors of a typical RPM. These results were compared against actual measurements at the RPM site, and shown to be within 10% of each other.

DEDICATION

To my family, for all the support and encouragement over the years.

AKNOWLEDGEMENTS

I would like to thank my committee chair, Dr. Craig Marianno, and my advisor Dr. Alexander Solodov for all their time, help, and patience in doing this research. Their comments and suggestions have aided this work along the way to completion. Thanks are also due to my committee members, Drs Dan Reece and Sunil Khatri, for their additional guidance and support. I would also like to thank Jeremy Osborne for his help on the transmission measurement experiments. Finally, thanks to my friends and colleagues for making my time at Texas A&M University a great experience. I would also like to recognize the sponsors of this research, Oak Ridge National Laboratory (ORNL).

NOMENCLATURE

EW	Energy Windowing
FWHM	Full-Width at Half Maximum
HEU	Highly Enriched Uranium
HPGe	High-Purity Germanium
ISOCS	In-Situ Object Counting System
MCA	Multichannel Analyzer
MCNP	Monte Carlo N-Particle
MDQ	Minimum Detectable Quantity
NAA	Neutron Activation Analysis
NaI	Sodium Iodide
NID	Nuclide Identification
NIST	National Institute of Standards and Technology
NNSA	National Nuclear Security Administration
NORM	Naturally Occurring Radioactive Material
Ø	Diameter
ORNL	Oak Ridge National Laboratory
PMT	Photomultiplier Tube
PNNL	Pacific Northwest National Laboratory
PVT	Polyvinyl Toluene
RDD	Radiological Dispersal Device

RPM	Radiation Portal Monitor
SANDIA	Sandia National Laboratory
SLD	Second Line of Defense
SNM	Special Nuclear Material

TABLE OF CONTENTS

Page

CHAPTER Page

LIST OF FIGURES

FIGURE Page

LIST OF TABLES

TABLE Page

CHAPTER I

INTRODUCTION

I.A. Motivation

Trafficking of radioactive material, particularly special nuclear material (SNM), has long been a worldwide concern. This concern has escalated in recent years because of the possibility of terrorists and rogue nations obtaining SNM for use in an explosive device or radiological dispersion device (RDD). The worldwide anxiety has prompted the United States government to invest large sums of money to interdict SNM smuggling. A portion of this money is used to install radiation portal monitors (RPMs) at border crossings and ports. The National Nuclear Security Administration's (NNSA) Second Line of Defense (SLD) is one such program that provides funding for this activity. SLD's has made it a priority to have radiation detection equipment at roughly 650 sites in almost 30 countries and 100 seaports by 2018. The NNSA requested a total of $2.5 billion for SLD for fiscal year 2012 with an additional $14.2 billion over the next 5 years.[1]

I.B. Problem Description

The choice of building materials surrounding an RPM site has a direct impact on detector background levels. RPMs are programmed to continually adjust the alarm threshold based on background counts. The minimum detectable quantity (MDQ) of an RPM depends on the background gamma radiation level. Minimizing background

radiation at the RPM installation site improves SNM detection. Materials around these sites, such as concrete and asphalt, consist of rock aggregate that contains naturally occurring radioactive material (NORM). In some cases, the gamma background contribution from NORM has been so high that the initial RPM setup required rebuilding; this included replacing the road and surrounding building material. This reconstruction greatly increased cost, delayed site installation, and allowed traffic to drive past without screening during reconstruction. This results in a need for a methodology that quickly and easily determines the specific activity and composition of building materials surrounding an RPM to reduce construction cost and time.

I.C. Overview of Research

The objective of this thesis is to develop a methodology that quickly and easily determines the specific activity and composition of building materials surrounding an RPM to estimate the background radiation level. This methodology required on site in-situ measuring and acquiring spectra from samples of the building material. In-situ measurements provide a more complete picture; however, this requires transporting expensive equipment to the site which in some instances is impossible. On the other hand, samples can be taken to a lab for measurement but may not provide all the information. Another piece of information needed is the elemental composition of the material. This information can be placed in radiation transport simulations to predict gamma interaction in the sample and detector. Although numerous methods can be used

to determine the elemental composition of a material, densitometry is proposed in this research.

To determine the specific activity of the asphalt surrounding a TSA Systems, Ltd. VM-250AG gamma portal monitor located at Oak Ridge National Laboratory (ORNL) the gamma emissions were measured using a collimated HPGe detector. The detector, asphalt and ground were modeled using Canberra Industries' In-Situ Object Counting System (ISOCS™) to generate an efficiency curve for the detector.[2] The resulting spectrum and efficiency curve were then used to quantify the specific activity of the asphalt concrete using GENIE 2000. This was also done with four asphalt samples to determine the viability of using samples in place of in-situ measurements.

To estimate the composition of the building materials at the site, the transmission rate of gamma rays through six samples of concrete and four samples of asphalt from ORNL were measured. Using Cs-137, Co-60, and Cd-109 sources with and without samples between the source and detector, the percent photon transmission was calculated for each sample and energy. The photon transmission through each sample was then used to estimate the elemental compositions of the six samples using densitometry equations. To complete the task, a code was written in C++ to solve the system of equations. The results of this code were compared against previous results obtained from neutron activation analysis.

To ultimately estimate the background signal in the VM-250AG RPM, MCNP 5 was used to calculate RPM MDQ from the measurements previously described. An input deck for MCNP for the RPM located at ORNL was modified by adding the surrounding

building material. The radiation source term for the asphalt was generated using the gamma spectroscopy analysis of the samples. The estimated elemental composition and measured density were then used to define the MCNP material card for concrete. Pulse height tallies were used to determine the total gamma ray count rate in each of the four gamma detectors in the RPM.

CHAPTER II

BACKGROUND

II.A. Radiation Portal Monitors & Gamma Rays

In response to the possibility of a nuclear threat by a terrorist and the risk it poses, the U.S. Government has developed "enhanced global nuclear detection architecture" in order to interdict SNM. This architecture consists of many layers that work in conjunction with each other to provide a comprehensive SNM threat detection system.[3,4] A key component of many of these layers is the use of RPMs. Although many different models and types of RPMs exist, they all perform the same basic function: to passively detect neutron and gamma radiation from pedestrian and vehicular traffic.

Passive material detection means that the radiation naturally emitted by the material is detected without having to induce that emission. Material emissions that RPMs can passively detect include: alpha, beta, gamma, neutron, and heat. Alpha, beta, and heat radiation are all easily attenuated and shielded from detection with only meager shielding. On the other hand, both neutrons and gammas penetrate material, making these types of radiation useful in detecting SNM. Neutron detection is attractive because neutrons are generally not emitted by NORM; however, SNM does not always emit neutrons, either. Conversely, most SNM emits gamma radiation, meaning the addition of gamma detection increases the chances of interdiction. In contrast to neutron background, natural gamma background is higher and is contingent on multiple factors: geographical location, altitude, surrounding material, weather, and time of day.

Gamma rays are electromagnetic radiation emitted by excited nuclei in order for them to reach the ground state after decaying. Once emitted, these particles mainly interact with matter in three ways: photoelectric effect, Compton Effect, and pair production. One or more of these interactions must take place in a detector in order for the incident gamma to register. Any of these interactions can occur within a detector; however, the probability of a specific interaction can dominate depending on the gamma energy and Z of the target material (Figure 1.)

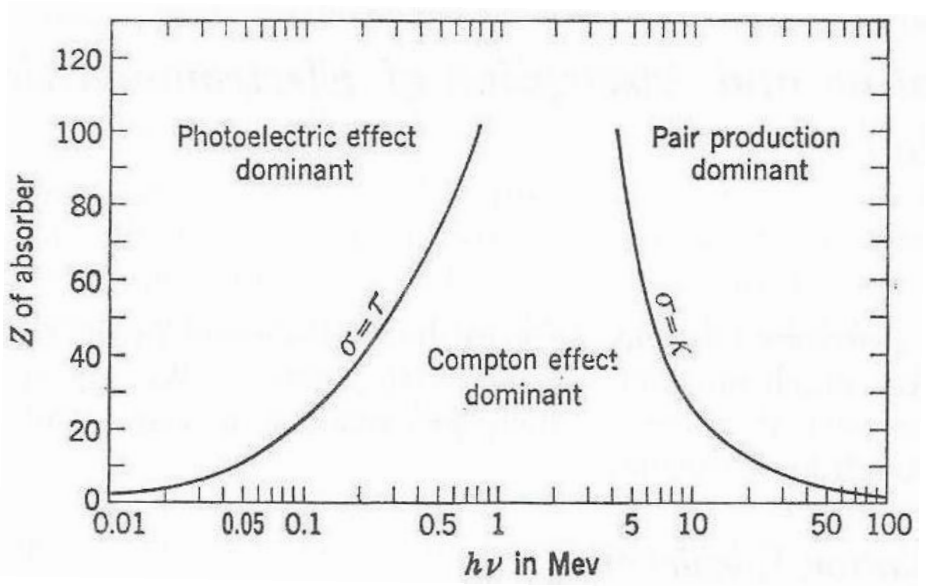

Figure 1. Relative Importance of the Three Major Types of Gamma Interactions and Their Relation to Energy and Z[5]

There are many different types of gamma detectors; however, the two preferred for gamma ray detection and spectroscopy are scintillation and semiconductor detectors. Both of these detectors take advantage of the electron band structure of the detection material. Electrons in atoms are arranged at discrete energy levels. When multiple atoms

assemble together, these discrete energy levels combine to create allowed and forbidden energy bands.

Scintillation detectors consist of a luminescent material and a device that detects the light given off by the material. The visible light is produced when an electron de-excites after being excited by incident radiation. When these electrons de-excite they emit a photon. In some scintillators, this process does not create visible light. In order to rectify this, impurities are added to the material. This creates more allowable energy states, and allows for the electrons to de-excite by emitting visible light. This visible photon produced in the scintillator then strikes a photocathode where it undergoes a photoelectric interaction and imparts all its energy to an electron. The electron next gets accelerated through a photomultiplier tube (PMT), hitting successive dynodes, creating more electrons and accelerating it further with each collision. Ultimately the electrons hit the anode, which creates an electrical pulse that compares proportionally in energy to the initial photon incident on the PMT.

Semiconductor detectors have a similar band structure to scintillators; however, in the case of scintillators, the band gap is much smaller. Additionally, semiconductor detectors have a voltage directly applied to them. The electric field generated from the applied voltage causes the electrons and holes to move in opposite directions; this allows for their charge to be collected. The collected charge then creates a pulse that relates proportionally to the energy of the incident radiation.

Runkle et al. states “there are three primary parameters that affect the performance of a gamma-ray spectrometer: energy resolution, intrinsic peak efficiency,

and absolute collection efficiency."[4] In addition to these three parameters, the cost of the detector should be considered when selecting a gamma spectrometer. Energy resolution measures the statistical dispersion of a mono-energetic gamma response peak and defined by the full width at half maximum (FWHM). FWHM means the width of the peak at half the height of the peak. The resolutions of three common gamma detection materials are shown in Figure 2. The HPGe detector has the thinnest peak, giving it the best resolution while PVT has a very broad peak, giving it the worst energy resolution of the three.

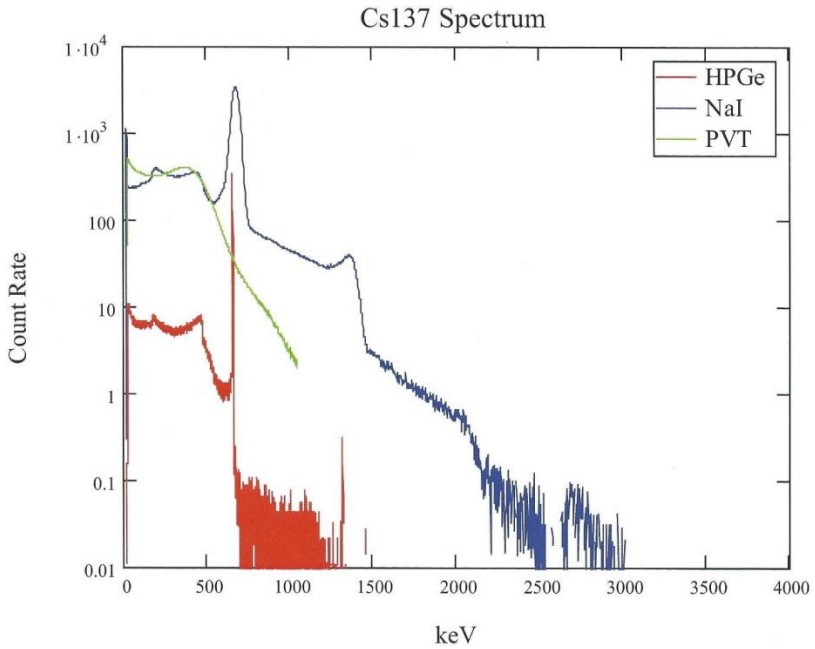

Figure 2. Detector Response Functions for HPGe, NaI, and PVT Spectrometers, Exposed to Cs-137 Gamma Rays[6]

The second figure of merit for gamma detectors is intrinsic efficiency. This is the ratio of the counts in a full energy peak to the number of gamma rays incident on the

detector, and relies on equivalent Z of the material. The peak efficiencies of the three detectors being compared are shown in Table I. Again, PVT is the worst, while the other two have similar efficiencies. This is due to the low average effective Z of PVT. As seen previously in Figure 1, a low Z value means Compton interactions more likely result in only partial energy deposition. NaI and HPGe have higher effective Z values, making full energy deposition by way of the photoelectric interaction more likely.

Absolute detection efficiency is the ratio of the total counts in a detector to the number of particles incident on the detector. For all three detector types, this value looks similar for detectors of the same size. This is because, in most practical cases, the detectors are thick enough that the total probability of interaction is high.

Table I. Intrinsic Peak Efficiencies for Various Sensors[4]

Detector	Dimensions (cm)	Volume (cm3)	Intrinsic peak efficiency	
			186 keV	1001keV
PVT	5.7 x 61 x 81	29000	0.0062	0.00061
NaI	5 x 10 x 40	2000	0.95	0.32
HPGe	d=6.2, t=7.8	120	0.94	0.29

Economic analysis of the three detector materials shows HPGe costs ten times more on a per volume basis than NaI, which in turn is roughly ten times more expensive than PVT.[4] It must also be noted that HPGe requires a much higher operation cost due to the necessity to keep it cooled to liquid nitrogen temperatures while PVT can be cheaply manufactured on a large scale.

The operating environment and detection capabilities along with the suggested uses can be found in the RPM operations manual. The RPM discussed and modeled for this project is the TSA Systems, Ltd. model VM-250AGN. This system contains two pillars both of which contain two 15 x 76 x 3.8 cm PVT scintillators and four 5 Ø x 91 cm, 2 atm, He-3 neutron detectors, along with the corresponding electronics and occupancy sensors. The master pillar also contains a battery, a battery charger, single channel analyzers, the system control circuitry, and communications ports.

When unoccupied, the VM 250AGN RPM continuously monitors the ambient gamma background. It does this by calculating the one-second count average over a user specified total background time of 20-120 seconds. The total background count time should be selected based on the estimated time it would take a vehicle to pass through the RPM.

A RPM's main alarm threshold setting, or N•Sigma alarm, can be easily understood. Once an RPM is occupied, it ignores the current background interval and collects counts in 200 ms intervals. The count rate over the interval is then compared to the alarm threshold.[7] The alarm threshold is determined using the following algorithm:

$$A_{th} = B + N\sigma_B \quad (1)$$

where: A_{th} is the alarm threshold,
B is the number of background counts,
N is a user-defined variable, and
σ_B is the standard deviation in the number of background counts. [7]

A graphical representation of this can be seen in Figure 3.

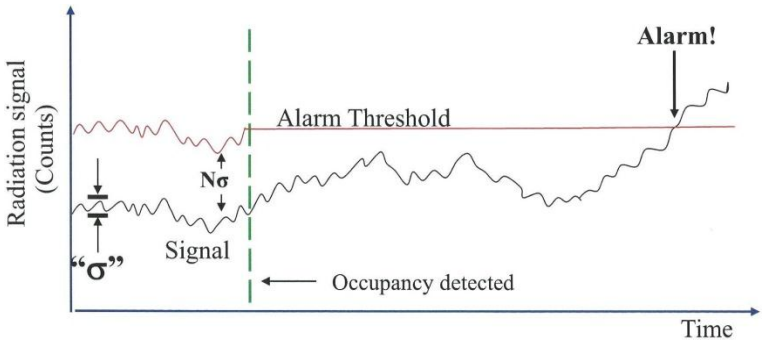

Figure 3: Determination of N•Sigma Alarm Threshold in an RPM.[6]

As seen in Eq. 1, the alarm threshold is dependent on B. A higher background increases the system's alarm level, which could lead to a higher quantity of material going undetected during transit. For a fixed counting time, the minimum detectable number of counts, N_S, is a function of the background described by the Currie Equation.[8] The Currie equation is derived assuming both false negatives and false positives occur 5% of the time. The Currie equation is:

$$N_S = 4.65\sqrt{B} + 2.71 \quad (2)$$

where: N_S is the number of signal counts, and
B_{avg} is the average background counts.

This equation can then be converted to MDQ for a particular energy by the following:

$$MDQ = \frac{N_S}{f\varepsilon T} \quad (3)$$

where: MDQ is the minimum detectable quantity of a specific energy,
f is the branching ratio of a specific energy gamma ray emitted per decay,
ε is the detector efficiency, and
T is the measurement time.

As seen in equations 2 and 3, both the alarm threshold and MDQ for an RPM are dependent on the background count rate. Thus the lower the background count rate, the lower the alarm threshold and the smaller the MDQ.

Additionally multiple functions and settings of the VM 250AGN RPM exist that can be adjusted by the user. This includes a high-low gamma alarm level can then be set to notify the user if the gamma count rates fall outside a given window. These numbers are static and set to expose system malfunctions or unnatural changes in background readings. Additionally, the RPM allows for energy discrimination in the detectors. For this project, the RPM was discriminated between 25 and 140 keV because the Compton Edge for highly enriched uranium (HEU) falls between these points. Another function of the VM-250AGN RPM is a "look back" and "hold in" capability. These expand the window of occupancy by a user specified time interval before and after the occupancy sensors are engaged. This prevents material at the front or rear of a vehicle from being ignored or affecting the background count rate.

II.B. Sources of Natural Background and Mitigation Method

There are many NORM which are classified in three general groups: cosmogenically produced, long lived isotopes, and daughters of long lived isotopes. The three main cosmogenically produced isotopes are Hydrogen-3, Berylium-7, and Carbon-14. There are 23 long lived, or primordial, isotopes with the most common being Potassium-40, Thorium-232, and Uranium-238. Table II list the 20 isotopes that occur

independent of any decay chain, their half lives, isotopic abundance, with their decay mode and energy.

Table II: Singly Occurring Primordial Radionuclides[9]

Nuclide	Half-Life (years)	% Isotopic Abundance	Decay Mode	Energy (MeV)
K-40	1.3×10^{9}	0.0118	Beta	1.32
V-50	6×10^{14}	0.25	Beta	-
Rb-87	4.7×10^{10}	27.83	Beta	0.273
Cd-113	9×10^{15}	12.3	Beta	-
In-115	5×10^{14}	95.7	Beta	0.49
Te-123	1.2×10^{13}	0.87	EC	-
La-138	1.1×10^{11}	0.09	Beta	0.27
Ce-142	$>5 \times 10^{16}$	11.1	Alpha	1.5
Nd-144	2.1×10^{15}	23.9	Alpha	1.83
Sm-147	1.1×10^{11}	15	Alpha	2.23
Sm-148	8×10^{15}	11.2	Alpha	1.95
Sm-149	$>10^{16}$	13.8	Alpha	<2.0
Gd-152	1.1×10^{14}	0.2	Alpha	2.14
Dy-156	2×10^{14}	0.06	Alpha	3 (?)
Lu-176	2.7×10^{10}	2.6	Beta	0.57, 0.31
Hf-174	2×10^{15}	0.17	Alpha	2.50
Ta-180	$>1.6 \times 10^{13}$	0.012	Beta	-
Re-187	5×10^{10}	62.5	Beta	0.0026
Pt-190	7×10^{11}	0.013	Alpha	3.16
Pb-204	1.4×10^{17}	1.48	Alpha	2.6

Most of the isotopes in Table II are of little interest due to their low isotropic abundance, low elemental abundance, or they do not emitting gammas. Thorium-232, Uranium-235, and Uranium-238 have radioactive daughters that build up and eventually reach secular equilibrium with their parents. These three decay chains with each isotopes half-life and decay modes are seen in Figure 4.

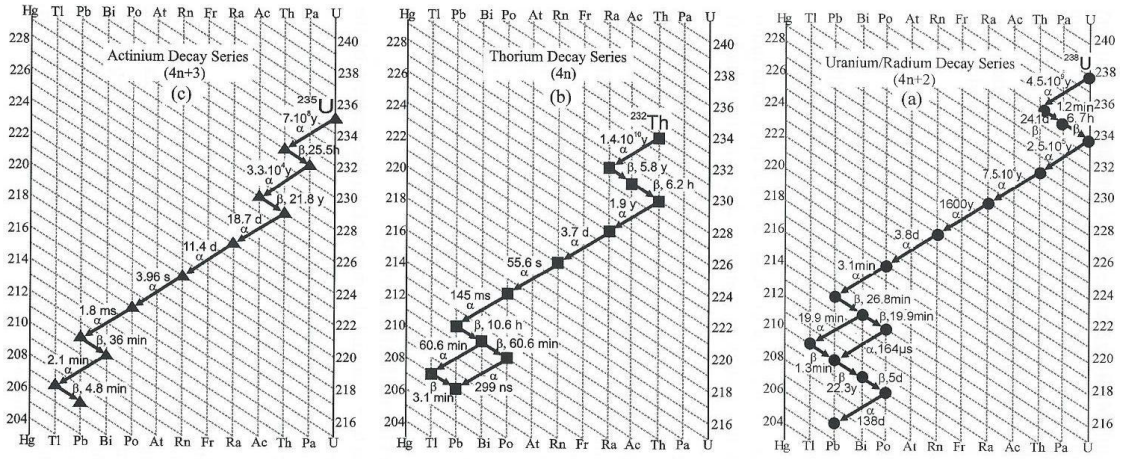

Figure 4: (a) Uranium/Radium, (b) Thorium, and (c) Actinium Decay Chains with Isotropic Half-lives and Decay Modes [10]

Like most of the primordial isotopes, a portion of these decay chain members do not emit gamma radiation. These naturally occurring isotopes are found in various concentrations throughout the world in natural materials like rock, soil, and organics.

With regards to roads and infrastructure, there is a variety of building materials employed, all of which contain various combinations of rock, soil, and organics. The two materials used primarily for roads and infrastructure are concrete and asphalt. The engineering term concrete includes any composite material comprised of aggregate and a binder, although commonly we use the term concrete to refer to concrete made with rock, gravel, or sand as an aggregate, cement binder, and water. In actuality, asphalt is a form of concrete and sometimes called asphalt concrete; it is derived from rock and gravel aggregate mixed with an asphalt (also called bitumen) binder. These two materials often get referred to by their binding material, cement and asphalt, although this reference is technically incorrect. For consistency and clarity in this thesis, these two

will be referred to as concrete and asphalt, respectively. Both of these building materials contain NORM material, the concentration of which depends on the constituents' origin and composition. Although low in concentration, the large volume of concrete and asphalt used can cause significant gamma emission by the material and cause problems in the detection of SNM by increasing the average background measured by the RPM.

There are a few methods for reducing the amount of NORM in building materials. Two obvious methods are to chemically remove the NORM or to use different raw material from sources that have low concentrations of NORM. The first of these methods requires a huge amount of time and money; therefore, it is rarely if ever done. The second can be done, but it can delay site installation and requires a method to quickly and effectively determine the impact raw materials will have on the RPMs. In some cases this has been done but it is generally reserved for when all other methods fail. More common methods are collimators, shielding, and wing plates.[11] Collimation places heavy material around the detector, which focuses the field of view of the detector. This reduces the amount of construction material and thus NORM seen by the detector, essentially putting blinders on the detector. Shielding acts in a similar fashion; metal plates are placed on the back of the RPM pillars that do not face traffic. This also reduces the amount of construction material seen by the detector and signal interference from traffic in neighboring lanes on the RPM site. The last method, installing wing plates, places metal plates on either side of the RPM. This tactic limits the distance the detector sees. When only one RPM column is used one large plate is placed where the second RPM column would be. A new method being explored is called energy

windowing (EW).[12] This method splits the gamma spectrum into windows and looks at the ratio of counts between windows. Ely et al have shown "that EW can indeed discriminate against NORM and maintain sensitivity to materials of interest, specifically SNM in certain scenarios."[12]

II.C. Use of Genie 2000

A software package from Canberra Industries known as Genie™ 2000 was employed in this project to analyze asphalt samples. Used in conjunction with an HPGe, this software has the capability to acquire and analyze spectra from a multichannel analyzer (MCA). This includes MCA control, spectral display and manipulation, basic spectrum analysis, and reporting of results.13 For an explanation of the software's features, one should refer to the *Genie™ 2000 Operations Manual*.[13] A more detailed guide to additional Genie™ 2000 analysis algorithms can be found in the *Genie™ 2000 Customization Tools Manual* from Canberra Industries.[13,14] This software package was chosen for its flexibility, ease of use, and customization features.

II.D. Efficiency Calibrations with ISOCS

An essential part of analyzing gamma spectra is to create an efficiency calibration for the detector and measurement geometry. This requires the development of a mathematical function that determines the probability that a particle of a specific energy will reach the detector, be detected, and can be applied over a wide range of gamma ray energies. With a mathematical detection efficiency determined as a function

of gamma energy, calculations can be made to accurately determine the activity of a sample. While it is possible to perform efficiency calibrations in a laboratory setting, this requires a reference source(s) of known activity to create a spectrum and measure the individual peak areas. This typically involves using an expensive calibration standard, and must be replicated for every source-detector geometry.[2] Additionally, this straight forward method is not achievable when one needs a calibration relevant to measurement of large and irregularly shaped items including an area of land.[15] Canberra's ISOCS™ software package helps reduce this high cost by applying mathematical techniques to determine the efficiency of an HPGe detector and radiological source geometry for various energies from 45 keV – 7 MeV. This requires an HPGe detector characterized by Canberra, the ISOCS™ software, and user-defined source geometry to produce an efficiency calibration file.

Characterization of the detector is performed by Canberra Industries using a National Institute of Standards and Technology (NIST) traceable point source and MCNP software. The HPGe detector is validated by modeling the NIST source in an MCNP deck. The detector efficiencies are then calculated using MCNP at quasi-random locations distributed around the detector. The detector's response characteristics for points within 1,000 m of the detector and over an energy range of 45 keV – 7 MeV are created from the MCNP results.[2]

The calibration software contains a set of mathematical templates that simulate various common shapes (boxes, cylinders, pipes, spheres, stacked boxes, stacked discs, Marinelli beakers, etc.). Each template allows input of user-defined parameters that are

necessary for efficiency calculation. This includes materials, density, and dimensions along with its position relative to the detector and any attenuators or collimators between the sample and detector. For the first run, the source region is subdivided into 1,024 voxels, and a point is quasi-randomly defined in each voxel. At each given energy level, the detection efficiency of each voxel is calculated, taking into consideration attenuation from absorbers, collimators, and shields. The total efficiency is then calculated by summing the voxels. Additional runs are performed, doubling the amount of voxels each time, until the results vary by less than the convergence criteria defined by the user.[16]

II.E. Determining Material Composition

The information related to material plays an important role for gamma interactions due to the fact that photons interact differently with each element. This difference in interaction means that to properly model an RPM system, the composition of the surrounding building materials is an important piece of information. Currently there is an almost endless list of methods to determine the elemental composition of a sample. These methods fall into five general categories: emission, fluorescence, transmission, mass, and ionization spectrometry.[17] Emission methods detect the characteristic nuclear radiation emitted from the atom. This can either be done actively where the atom is excited by another form of radiation or passively where the natural radiation is measured. This excitation can be done by heat or in the case of Neutron Activation Analysis (NAA), neutrons. In fluorescence spectroscopy, a light source excites the material's atoms and their characteristic fluorescence, or light emitted, gets

measured. Transmission impinges a beam of monoenergetic particles and based on the attenuation, the elements can be determined. Mass spectroscopy accelerates ions generated by the material through a magnetic field; this causes the different ions to travel different paths based on mass and charge of the ion. Ionization spectrometry uses a finely tuned laser to selectively ionize a specific elements; the current generated by the collection of these ions is then measured. All of these methods have advantages and disadvantages, most of which relate to sample preparation, access to equipment, time involved, cost, and sensitivity. For this research, the transmission method of densitometry was selected because it required little sample preparation, could be done with available gamma detectors and small check sources, took minimal time and money, and provided a reasonable estimate for low Z materials with many constituents without requiring special treatment.

Densitometry determines a material's density by the transmission of gamma rays through the material. In some cases, gamma-ray transmission measurements can provide information about the composition of a sample as well as bulk density.[18] According to Evans[5], it is useful to use the mass attenuation instead of linear attenuation coefficient because Compton attenuation is roughly the same for all materials when measured in terms of mass attenuation coefficients. The uncollided gamma flux through a sample is determined by the following equation:

$$I = I_0 e^{-\frac{\mu}{\rho}\rho x} \qquad (4)$$

where I is the uncollided photon flux exiting the sample,
I_0 is the uncollided photon flux entering the sample,
μ/ρ is the mass attenuation coefficient (dependent on Z and energy), and

ρ is the sample density, and
x is the sample thickness.

Equation 4 is for samples of a single element but this experiment used cement and asphalt, which are mixtures of several elements. In order to calculate the mass attenuation coefficient for such a mixture the following equation is used:

$$\frac{\mu}{\rho} = \sum \left(\frac{\mu}{\rho}\right)_i \omega_i \tag{5}$$

where: μ/ρ is the total mass attenuation coefficient,
$(\mu/\rho)_i$ is the mass attenuation coefficient of element i, and
ω_i is the weight fraction of element i.

Combining and rewriting equations 4 and 5:

$$\sum \left(\frac{\mu}{\rho}\right)_i \omega_i = -\frac{\ln\left(\frac{I}{I_0}\right)}{\rho x} \tag{6}$$

If transmission experiments are done using multiple energies, the mass fractions of the constituent elements can be computed using Equation 6 if all the other variables are known.

II.F. Computational Tools

Computational tools were used to aid in this research because they allowed for the extension of the scope and complexity of the problems needed to be solved by numerical methods. This meant extremely large and complex problems with uncertainties were able to be solved in a short amount of time. The two computational tools used for this research were the C++ programming language and MCNP. A program written in C++ was used to specify the constraints of the system and write these

constrains as instructions for the computer. The computer then could use these instructions to iteratively solve the system.

MCNP was used because it allowed a complex, 3D model of the actual system. This included the use of distributed source terms with independent energy distribution probabilities, along with particle tallies over multiple volumes. Additionally MCNP has built-in access to tens of thousands of continuous-energy nuclear and atomic data libraries, which allows necessary information to be obtained for a variety of inputs. MCNP also allows for a large number of variance reduction methods that when employed can lower the computational time and improve relative errors.[19] For this research it was possible to model an RPM located at ORNL and easily modify the surrounding building material. This model then provided the detector response.

CHAPTER III

EXPERIMENTS AND SIMULATIONS

III.A. Procedure

The objective of this research was to develop a methodology to quickly and cost-effectively predict the gamma background in an RPM setup by determining the specific activity and composition of building materials surrounding the RPM. This required measuring the gamma ray emission of building material in-situ and in the lab. The detector and sample being measured were then modeled using ISOCS™ to generate a detector efficiency curve.[2] The measured gamma spectrum, calculated efficiency curve, and a user created Nuclide Identification (NID) library were then used to quantify the activity of the asphalt concrete using GENIE 2000.

The other component needed is the material composition of the material in the model to properly account for gamma interactions. To estimate the material composition of the building materials at the test site, the transmission rate of gamma rays through the material samples was measured. This was done using Cs-137, Co-60, and Cd-109 sources, with and without samples between the source and detector. The ratio of full energy counts was then calculated for each sample and energy, and was then used to estimate the elemental compositions of the samples using the densitometry equations; these equations were solved by a C++ code. The results of this code were compared against previous results obtained from NAA.

These two pieces of information were then inputted into an MCNP 5 deck modeling the VM-250AG RPM located at ORNL. Pulse tallies over different energy windows were used to determine the total gamma ray count rate in each of the four detectors in the RPM. These were then compared to previous simulations using the composition from NAA and measured data.

III.B. Gamma Ray Background Measurements

Four asphalt samples were acquired from ORNL for the experimental measurements as a part of this project. Each sample came from the same asphalt slab. A photo of the samples can be seen in Figure 5.

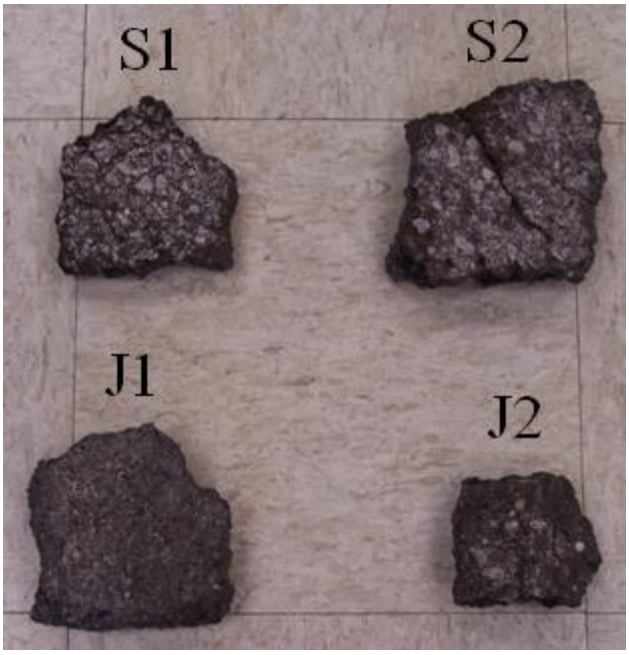

Figure 5: Photo of the Four Asphalt Samples Used for This Research

In order to determine the density of the samples, the dimensions were measured with a digital caliper. As can be seen in Figure 5, the samples do not take any standardized shape; this meant that the angles between sides needed to be measured with a protractor. Based on the results of the measurements, the volume of the samples was then calculated. Additionally, sample masses were needed to calculate sample density. The mass was measured using a digital balance. The density of the samples was subsequently calculated from the calculated volume and mass. The average thickness of the samples is 4.11 cm, and the average density is 1.628 g cm^{-3}. The data obtained from all the measurements is shown in Table III.

Table III. Characteristics of Experimental Asphalt Samples

Sample	Cross Sectional Area (cm^2)	Thickness (cm)	Volume (cm^3)	Mass (g)	Density (g/cm^3)
OR-S1	99.04	3.30	327	536.2	1.64
OR-S2	137.9	4.57	630	1099.2	1.74
OR-J1	118.8	4.57	543	887.0	1.63
OR-J2	60.13	4.01	241	359.7	1.49

To calculate the specific activity of the samples the gamma emission of each was measured. This measurement was taken using a shielded, energy calibrated Canberra BEGE 8494 HPGe detector. The gamma spectra were acquired using Genie™ 2000 software and an 8,192 channel Canberra Inspector-2000 MCA. Prior to counting any samples, a 24 hour live-time gamma background measurement was taken. Following the background count, a sample was placed 8.5 cm away from the detector face on a hollow

riser with thin plastic walls. A photo of the experimental geometry, including the detector, sample, and lead vault is shown in Figure 6.

Figure 6: Photos of the Experimental Geometry, Including the Detector, Sample, and Vault, Used for the Sample Gamma Ray Background Activity Measurements

A 24-hour gamma measurement of the sample was done for each of the four samples. Additionally, a 96-hour gamma measurement of sample S2 was taken to determine if this improved the detection capability and statistics. All measurement times are quoted as live time. The gamma spectra for all 4 samples, as well as the background measurement, can be found in Appendix A.

Finally, in-situ measurements were taken at ORNL. A collimated Canberra Industries broad energy model BE3825 HPGe detector coupled with an 8,192 channel Canberra 1300 InSpector 2000 DSP Portable MCA was used. The experimental setup can be seen in Figure 7. The energy calibrated detector was placed between the two

RPMs. It was rotated to face downward, so that the detector face stood 73.34 cm above the asphalt. A one hour live-time gamma background measurement was taken with the collimator closed. A seven hour live-time gamma measurement was taken, with the collimator fully opened, the two spectra can also be found in Appendix A.

Figure 7. Photo of the in-situ Setup, Including the Detector, Collimator, and Cart, Used for the in-situ Gamma Ray Background Activity Measurements

III.C. Efficiency Calibration Using ISOCS

To determine the efficiency calibrations for each detector set-up, geometry models were generated for each asphalt sample using ISOCS™ software package in conjunction with the generic detector characterization supplied by Canberra for a model BE3825 HPGe detector. The simple box template used to model the asphalt samples is shown in Figure 8.

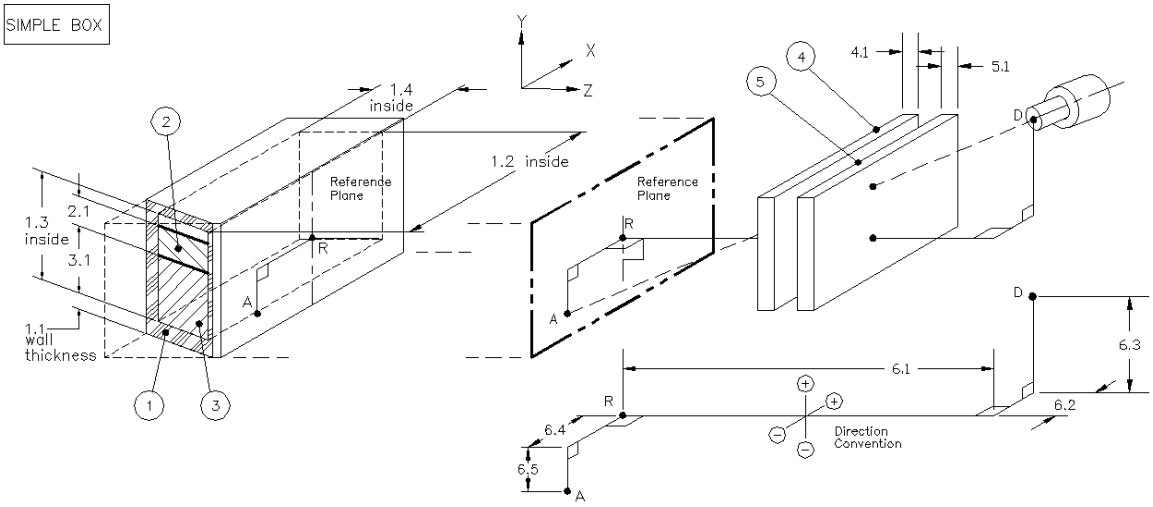

Figure 8: ISOCS™ Simple Box Template Used for Generation of the Efficiency Calibration Files[20]

In Figure 8, R refers to the source reference point (this is the center of the front of the sample) D is the detector reference point (the center of the detector endcap) and A is the detector aiming point, Object 1 is the asphalt box itself and Dimension 1.1 is the thickness of the container walls. Although the sample does not have a nonradioactive outer layer, this dimension is required by the program. This dimension was set to 10^{-5} cm for all samples as to not significantly affect their attenuation characteristics. Dimensions 1.2, 1.3, and 1.4 are the width, height, and depth of the sample. Due to the fact that these samples are not regular rectangles, an approximate rectangle must be determined by calculating the size of two regular rectangles, one that is inscribed within the sample and one that is circumscribed. The approximate sample size was then determined so that the cross sectional area is the same as the actual sample, and the percent difference between the sides of the circumscribed and inscribed rectangles in each direction are the same.

An illustration of this method can be seen in Figure 9, and the approximate sample dimensions are seen in Table IV. The thickness was directly measured for each sample.

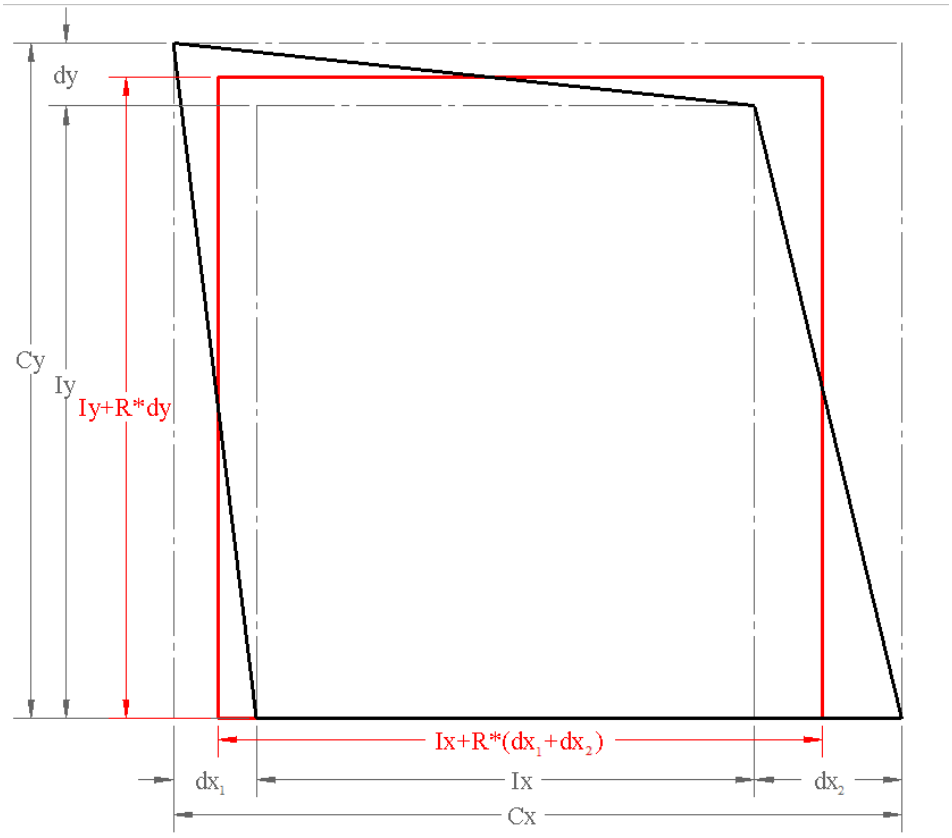

Figure 9: Method for Determining a Regular Rectangle Approximation for Asphalt Samples

Table IV: Regular Rectangle Approximation Dimensions for Asphalt Samples

Sample	R	Width (cm)	Height (cm)	Thickness (cm)
OR-S1	.590	10.3	9.63	3.30
OR-S2	.607	11.9	11.6	4.57
OR-J1	.643	10.6	11.2	4.57
OR-J2	.595	8.18	7.36	4.01

Objects 2 and 3 of Figure 8, represent the top and bottom portions of the source, respectively. For these measurements, the entire sample was treated as the upper portion source, setting dimension 2.1 the same as 1.3 while dimension 3.1 was set to 0. Objects 4 and 5 are for absorber plates that may be present between the detector and the source. Since no absorbers were used in the experimental geometry, these dimensions were left blank. The input parameters for sample S1 are seen in Table V, and the remainder can be found in Appendix B.

Table V: ISOCS™ Efficiency Calibration Input Parameters for Asphalt Sample S1

No.	Dimensions (cm)					Material	Density	Rel.
	d.1	d.2	d.3	d.4	d.5		(g cm-3)	Conc.
1	0.00001	10.29	9.63	3.30	N/A	asphalt	1.64	N/A
2	9.63	N/A	N/A	N/A	N/A	asphalt	1.64	1
3	0	N/A	N/A	N/A	N/A	asphalt	1.64	0
4	0	N/A	N/A	N/A	N/A	(none)	0	N/A
5	0	N/A	N/A	N/A	N/A	(none)	0	N/A
6	8.50	0	0	0	0	N/A	N/A	N/A

Object 6 defines the relation between the center of the sample and the detector face as well as the point on the sample where the detector is facing. Dimension 6.1 is the distance between these points, the detector and the sample, and was set to 8.5 cm for all samples since the experimental geometry did not change between measurements. Dimensions 6.2, 6.3, 6.4, and 6.5 define the translation of the detector and source in the x- and y-directions. In every case, the center of the sample lined up exactly with the center of the detector, therefore these dimensions were set to 0.

The material composition for asphalt was defined based on the suggested elemental composition of "asphalt concrete" from Pacific Northwest National Lab's (PNNL) Compendium of Material Composition Data for Radiation Transport Modeling.21 Measured densities of each sample were used in sample material descriptions.

An efficiency calibration file was also generated for the in-situ measurement at ORNL following the procedure for measuring soil activity or contamination suggested by the ISOCS manual.[2] The suggested procedure makes use of the rectangular plane template seen in Figure 10 to model the ground and set the height, width, and length of Object 1 to 20 m.

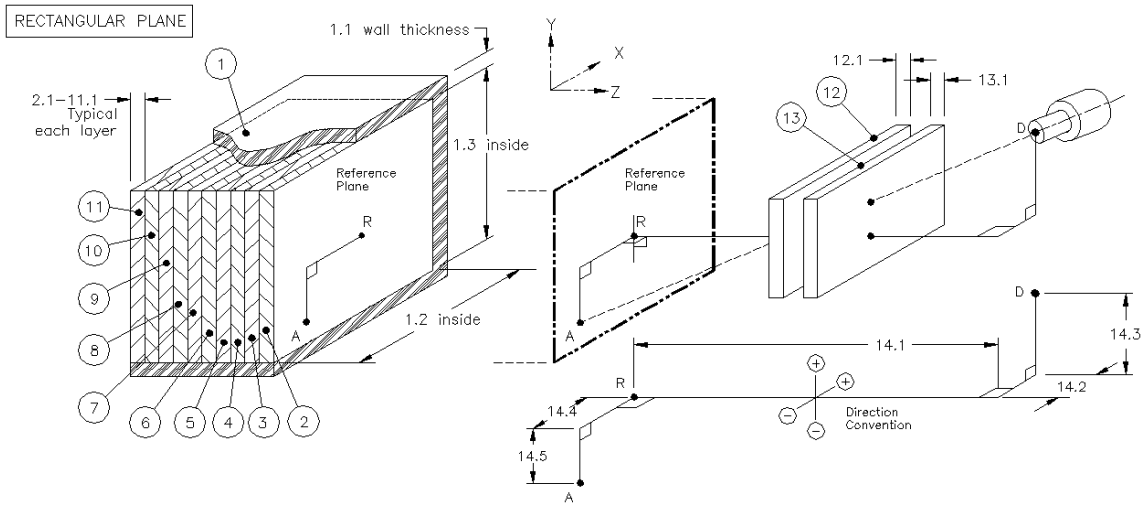

Figure 10: ISOCS™ Rectangular Plane Template Used for Generation of the Efficiency Calibration Files[20]

For this template, Object 1 represents the side walls around the source layers. Dimension 1.1 was again set to 10^{-5} cm, and dimensions 1.2 and 1.3 were set to 20 m.

Objects 2-11 are the possible radioactive source layers. For this measurement, three layers were assumed: asphalt (Object 2), gravel (Object 3), and soil (Object 4). The asphalt and gravel were assumed to be equally radioactive while the soil was assumed to be nonradioactive. This assumption was to reduce computational time and resulted in the same efficiency as a model with the soil equally as radioactive as the gravel and asphalt. Dimension 2.1 was set to the thickness of the asphalt (5 cm), dimension 3.1 was set to the thickness of the gravel layer (10 cm), and dimension 4.1 was set to 20 m. The thickness of the remaining layers was set to 0.

In this template, Object 14 defines the source-detector position, as Object 6 did in the previous template. Dimension 14.1 is the distance between points—the detector and the sample—and was set to 73.34 cm for the in-situ measurement. The remaining dimensions were set to 0 as advised in the ISOCS operations manual.

The average density of the asphalt samples was used for the density of Objects 1 and 2. The material composition of both objects was again defined based on the suggested elemental composition of asphalt concrete.[21] The density and composition for rock (average of 5 types) from the PNNL Compendium was used for Object 3. This is an average of basalt, granite, limestone, sandstone, and shale. Object 4's density and composition came from the compendium's values for Earth, U.S. Average. These material assumptions have been shown to be reasonable for an efficiency calculation because dealing with a near infinite source area the other variables minimally affect the efficiency curve.[22] The material definition and density for the other objects were left blank. The input data can be seen in Table VI.

With the input parameters defined, efficiency data points were generated. The resultant file was used to calculate the background activity of the asphalt in-situ.

Table VI: ISOCS™ Efficiency Calibration Input Parameters for in-situ Asphalt

No.	Dimensions (cm)					Material	Density	Rel.
	d.1	d.2	d.3	d.4	d.5		(g cm-3)	Conc.
1		2000	2000	N/A	N/A	asphalt	1.72	N/A
2	5	N/A	N/A	N/A	N/A	asphalt	1.72	0.5
3	10	N/A	N/A	N/A	N/A	rock	2.66	0.5
4	2000	N/A	N/A	N/A	N/A	earth	1.52	0
5	0	N/A	N/A	N/A	N/A	(none)	0	0
6	0	N/A	N/A	N/A	N/A	(none)	0	0
7	0	N/A	N/A	N/A	N/A	(none)	0	0
8	0	N/A	N/A	N/A	N/A	(none)	0	0
9	0	N/A	N/A	N/A	N/A	(none)	0	0
10	0	N/A	N/A	N/A	N/A	(none)	0	0
11	0	N/A	N/A	N/A	N/A	(none)	0	0
12	0	N/A	N/A	N/A	N/A	(none)	0	N/A
13	0	N/A	N/A	N/A	N/A	(none)	0	N/A
14	73.342	0	0	0	0	N/A	N/A	N/A

III.D. Asphalt Background Activity

Once the efficiency calibration files were generated, it was possible to calculate the background activity for each asphalt sample as well as the in-situ asphalt activity. GENIE 2000 was used to find and determine the area under each peak in the spectrum. The peak areas from the background measurement were then subtracted from the gross peak areas. Next the ISOCS™ efficiency calibration file for the sample was applied to the spectrum. The gamma peaks were identified in addition to the isotopes' weighted mean activities.

To perform the nuclide identification, a custom library was created within GENIE by compiling all the non-cosmogenic NORM isotopes that emit gamma or x-rays. This list was then reduced to only include those isotopes with gamma or x-ray lines with energies greater than 40 keV and branching ratios greater than 1%; this was done because below 40 keV, the gamma peaks are lost in noise and gammas with branching ratios under 1% occur too infrequently to be observed. In addition to the gamma energies and branching ratios, the specific activity and half-life of each isotope was input into the library.

III.E. Radioactive Source Term for MCNP

Once the background activity of each sample was determined, the MCNP source term for each was calculated. Using the activity of each nuclide found in the sample, the gamma emission rate was calculated. The gamma energies identified by the GENIE 2000 software were listed along with the activity of their corresponding nuclide and respective yields. The emission rate for each gamma energy line, the total gamma emission rate, and fractional emission rates were calculated using Equations 7-9, respectively.

$$\varepsilon_{E,i} = y_E \, A_{tot,i} \quad (7)$$

$$\varepsilon_{tot} = \sum_{i=1} \varepsilon_{E,i} \quad (8)$$

$$f_{E,i} = {}^{\varepsilon_{E,i}}/_{\varepsilon_{tot}} \quad (9)$$

where $\varepsilon_{E,i}$ is the gamma emission rate at energy E for nuclide i,
y_E is the radiative yield of the gamma ray at energy E,
$A_{tot,i}$ is the total activity of nuclide i in the slab,
ε_{tot} is the total gamma emission rate of all nuclides in the slab, and
$f_{E,i}$ is the fractional emission rate of the gamma ray at energy E for nuclide i.

III.F. Concrete Sample Gamma Transmission

The last component required to determine the gamma interactions in the RPM is the elemental composition of the material surrounding the devices. To estimate the elemental composition of the surrounding building materials, the transmission of gamma rays through the material samples was measured; this was done using Cd-109, Cs-137, and Co-60. The energies that correspond to each nuclide are documented in Table VII. To calculate the percent transmission through each, a check source of each isotope was placed a fixed distance from an HPGe detector. The photopeaks were then measured with and without samples between the source and detector. The ratio of counts between the photopeaks was then calculated for each sample and energy; the experimental setup can be seen in Figure 11.

The area under the full energy peak was calculated in both spectra and the ratio between the two areas was determined; this ratio is the gamma transmission. This process was repeated with each source for all samples. The calculated transmissions for concrete are shown in Table VIII and for asphalt in Table IX. It should be noted that the

transmission results are not listed for Cd-109's 88 keV photons because the low energy and source activity made the photon indistinguishable from the background.

Table VII: Source Information

Nuclide	Energy (keV)	Half Life (years)	Emission Rate (%)
^{109}Cd	88.03	1.264	3.70
^{137}Cs	661.66	30.08	85.1
^{60}Co	1173.24	5.275	99.97
	1332.50	5.275	99.99

Figure 11: Photo of the Experimental Setup of the Concrete Transmission Measurement

Table VIII: Percent Transmission through the Six Concrete Samples

	88.03 keV	661.65 keV	1173.24 keV	1332.50 keV
F1	34.8±0.88	66.44±0.55	69.29±0.91	73.23±0.99
F2	32.7±0.85	65.31±0.54	71.42±0.93	72.82±0.99
G1	31.5±0.85	62.00±0.52	67.96±0.90	69.36±0.96
G2	32.4±0.85	62.68±0.53	68.75±0.90	70.01±0.96
L1	34.6±0.88	65.28±0.54	71.17±0.93	73.58±1.00
L2	35.1±0.88	65.93±0.54	71.21±0.92	71.83±0.98

Table IX: Percent Transmission through the Four Asphalt Samples

	88.03 keV	661.66 keV	1173.24 keV	1332.50 keV
ORNL-J1	N/A	59.19±0.01	63.54±0.04	70.58±0.06
ORNL-J2	N/A	47.52±0.28	56.73±0.04	60.98±0.05
ORNL-S1	N/A	46.53±0.01	51.42±0.03	58.74±0.05
ORNL-S2	N/A	51.52±0.01	59.29±0.04	64.80±3.15

III.G. Concrete Composition Determination Code

As stated previously Equation 6 is the key to densitometry, this equation is as follows:

$$\sum \left(\frac{\mu}{\rho}\right)_j \omega_j = -\frac{\ln\left(\frac{I}{I_0}\right)}{\rho x}$$

where: $(\mu/\rho)_j$ is the mass attenuation coefficient of element j, and
ω_j is the weight fraction of element j.
I is the uncollided photon flux exiting the sample,
I_0 is the uncollided photon flux entering the sample,
ρ is the sample density, and
x is the sample thickness.

Applying the equation at multiple energies results in a set of equations that can be represented by the following matrix:

$$\begin{bmatrix} \left(\frac{\mu}{\rho}\right)_{11} & \left(\frac{\mu}{\rho}\right)_{12} & \cdots & \left(\frac{\mu}{\rho}\right)_{1J} \\ \left(\frac{\mu}{\rho}\right)_{21} & \left(\frac{\mu}{\rho}\right)_{22} & \cdots & \left(\frac{\mu}{\rho}\right)_{2J} \\ \vdots & \vdots & \ddots & \vdots \\ \left(\frac{\mu}{\rho}\right)_{I1} & \left(\frac{\mu}{\rho}\right)_{I2} & \cdots & \left(\frac{\mu}{\rho}\right)_{IJ} \end{bmatrix} \begin{bmatrix} \omega_1 \\ \omega_2 \\ \vdots \\ \omega_J \end{bmatrix} = \begin{bmatrix} -\frac{\ln\left(\frac{I}{I_0}\right)}{\rho x}_1 \\ -\frac{\ln\left(\frac{I}{I_0}\right)}{\rho x}_2 \\ \vdots \\ -\frac{\ln\left(\frac{I}{I_0}\right)}{\rho x}_I \end{bmatrix} \quad (10)$$

The previous set of equations represents an ill-posed problem, as there can be more unknowns than equations while there are also various uncertainties built into every number. One method to solve the set of equations was developed by Griffin et al at

SANDIA national labs, starting with an initial guess and iteratively improving upon this guess by using the following equations:[22]

$$-\frac{\ln\left(\frac{I}{I_0}\right)}{\rho x}_i = A_i \tag{11}$$

$$A_{ij}^k = \left(\frac{\mu}{\rho}\right)_{ij} \omega_j^k \tag{12}$$

$$A_i^k = \sum_{j=1}^{J} A_{ij}^k \tag{13}$$

$$E_i^k = \frac{\mathrm{abs}\left(A_i - A_i^k\right)}{A_i} \tag{14}$$

$$E_{total}^k = \sum_{i=1}^{I} E_i^k \tag{15}$$

$$W_{i1}^k = \frac{A_{i1}^k}{A_i^k} \tag{16}$$

$$W_{ij}^k = \frac{1}{2}\frac{\left(A_{ij}^k - A_{ij-1}^k\right)}{A_i^k} \text{ for } j=2,\ldots,J \tag{17}$$

$$R_i^k = \frac{A_i}{A_i^k} \tag{18}$$

$$C_j^k = \frac{\sum_{i=1}^{I} W_{ij}^k \ln\left(R_i^k\right)}{\sum_{i=1}^{I} W_{ij}^k} \tag{19}$$

$$\omega_j^{k+1} = \omega_j^k \exp\left(C_j^k\right) \tag{20}$$

where: $(\mu/\rho)_j$, ω_j, I, I_0, ρ, and x are the same as in Eq. 7,

A_i is the measured total mass attenuation coefficient for energy I,

A_{ij}^k is the estimated fraction of total mass attenuation coefficient for energy i, iteration k, and element j,

A_i^k is the estimated total mass attenuation coefficient for energy i and iteration k,

E_i^k is the error between the measured to estimated total mass attenuation coefficient for iteration k,

E_{total}^k is the total error of the system of equations for iteration k,

W_{ij}^k is the weighting function for energy i, and element j,

R_i^k is the ratio of measured to estimated total mass attenuation coefficient for iteration k, and

C_j^k is the correction function for element j, and iteration k.[23]

This series of equations is looped through in iterations until $E_{total}^{k+1} \geq E_{total}^{k}$ when the iterations stop and ω_j^k is the final value for ω_j. Using C, Equations 13-22 are written in a loop to quickly solve for ω_j.

III.H. MCNP Simulations

Once the estimated concrete composition is calculated, an MCNP simulation was conducted for each concrete sample. The MCNP simulation was done to determine if the estimated composition from densitometry measurements proved similar to the material attenuation data as the composition determined through NAA by Ryan.[25]

A deck was created to model the concrete transmission experiment as explained in Section III.E. A material card was then created for each concrete sample based on the densitometry estimation and on the NAA results. The general MCNP deck and all the material cards can be seen in Appendix B. The number of counts reaching the detector was recorded using an F1 current tally over the face of the detector. Energy bins were used around the region of interest for each source nuclide. The energy bins changed depending on the check source used. A total of 10^8 particles were started for each simulation. After running each deck, the ratio of counts in the detector with and without a sample present was determined for each sample. The results are shown in Table X.

Table X: Simulated Transmission through a Sample of Estimated Composition

Energy (keV)	88.03	661.66	1332.5
F1	32.90±0.43	62.81±0.25	71.83±0.24
F2	30.59±0.46	61.25±0.25	70.52±0.24
G1	30.66±0.46	59.60±0.26	69.02±0.24
G2	33.31±0.43	61.79±0.26	70.90±0.24
L1	32.53±0.43	62.5±0.25	71.56±0.24
L2	34.96±0.41	64.52±0.25	73.09±0.24

To estimate the total gamma ray count rate in each of the four detectors in the RPM, the specific activity and elemental composition of the material surrounding the RPM were inputted into an MCNP deck modeling the RPM setup at ORNL. Pulse tallies over different energy windows were used and compared to simulations using the composition from NAA as well as measured data.

CHAPTER IV

RESULTS AND DISCUSSION

IV.A. Calculated Asphalt Background Activity

The specific activities of the individual isotopes identified in each sample are given in Table XI where BDL signifies the isotope was below detectable limits in the sample. The isotopes are grouped by decay chain to determine if the identified isotopes are in secular equilibrium with their entire decay chain. The decay chain combined averaged activities are seen in Table XII.

Table XI: Specific Activities of the Background Isotopes in the Asphalt Samples

	Decay Chain	BR	J1 (μCi/kg)	J2 (μCi/kg)	S1 (μCi/kg)	S2 (μCi/kg)	in-situ (μCi/kg)
K-40	N/A	1	568±49	826±73	509±60	634±47	6510±337
Tl-208	Th-232	0.36	13.4±2.5	BDL	13.0±3.4	7.53±1.89	BDL
Bi-212	Th-232	1	BDL	BDL	BDL	BDL	204±88
Pb-212	Th-232	1	20.3±2.7	27.4±5.2	31.3±5.3	31.8±3.0	235±21
Ac-228	Th-232	1	BDL	BDL	22.0±9. 9	BDL	169±22
Pb-210	U-238	1	108±63	BDL	308 ±78	259±64	982±352
Bi-214	U-238	1	44.0±5.6	68.6±11.7	47.6±8.5	42.5±4.9	292±15
Pb-214	U-238	0.9998	63.8±5.0	52.8±9.2	61.8±6.0	59.8±4.9	302±22
Ra-226	U-238	1	153±48	324±84	BDL	178±43	BDL
Th-234	U-238	1	BDL	BDL	103±54	BDL	BDL

Table XII: Decay Chain Averaged Specific Activities of the Background Isotopes in the Asphalt Samples

	J1 (μCi/kg)	J2 (μCi/kg)	S1 (μCi/kg)	S2 (μCi/kg)	in-situ (μCi/kg)
K-40	568±49	826±73	509±60	634±47	6510±337
Th-232	16.3±1.8	BDL	17.5±2.7	13.9±1.6	159±11
U-238	56.1±3.7	70.7±6.9	62.3±4.8	55.5±3.4	298±13

Although some members of the decay chain have a specific activity within ±2σ of the averaged activity of the entire chain, outliers and some missing members skew the decay chain's activity. It should also be noted that although theoretically in secular equilibrium, elements are transported through materials differently; this causes inconsistencies in isotope activity. Additionally, the data indicates that the specific activities of the same isotope are within at least ±2σ of the average of them all for isotopes seen in the sample, the exception being Pb-212 in sample J1. This discrepancy, along with the fact that not all isotopes were detected, can be explained by the samples coming from a heterogeneous source. Due to this and the fact as stated above that the elements are carried through the material differently, certain samples will have higher concentrations of elements than others. These two discrepancies show that the assumption of secular equilibrium and averaging the activity of the entire decay chain is not a viable method of analysis.

The discrepancy between the sample analyses versus in-situ measurements is most likely explained by the fact that the asphalt in the field has natural material behind it, mostly gravel and soil. Additionally, the field source is much larger, allowing for a better averaging of the heterogeneity of the gamma emission from the materials. Based

on the discrepancy between the results, the in-situ measurement was chosen for further analysis in this work. Using Equations 7-9, an MCNP source card was generated from the in-situ measurements and can be seen in Figure 12.

```
SI15     L 0.04654 0.07281 0.07481 0.07482 0.07497 0.07710
           0.07711 0.08437 0.08477 0.23863 0.29522 0.33832
           0.35193 0.51000 0.51077 0.58319 0.60931 0.72733
           0.76836 0.91120 0.96897 1.12029 1.23811 1.46081
           1.76449 1.84742 2.20421 2.61451
SP15     D 0.00653 0.00117 0.00599 0.00891 0.00195 0.00996
           0.01490 0.00187 0.00069 0.02540 0.02829 0.00657
           0.05467 0.00012 0.01317 0.04952 0.06880 0.00389
           0.00737 0.01503 0.00920 0.02273 0.00900 0.54198
           0.02359 0.00313 0.00746 0.05811
```

Figure 12: MCNP Source Term from the in-situ Asphalt Measurement

IV.B. Composition of Concrete and Asphalt

Inputting the measured density, thickness, and percent transmission of the six concrete and four asphalt samples in the densitometry solver program to estimate the solution to the densitometry equations, the estimated composition of the samples was calculated. Table XIII & Table XIV show the estimated composition of the samples.

Table XIII: Estimated Weight Fraction of Concrete Sample

	F1 ±20.62%	F2 ±21.18%	G1 ±20.18%	G2 ±20.22%	L1 ±21.64%	L2 ±19.62%
H	0.033711	0.017612	0.080161	0.124999	0.029552	0.119111
C	0.003921	0.001958	0.009936	0.016375	0.003369	0.016020
O	0.531250	0.549496	0.510624	0.399632	0.614243	0.283515
Na	0.014077	0.014511	0.013599	0.010649	0.016252	0.007545
Mg	0.001097	0.001282	0.000886	0.000677	0.001340	0.000492
Al	0.017120	0.021241	0.012496	0.010184	0.021627	0.008039
Si	0.348819	0.313240	0.346864	0.408146	0.245125	0.528034
K	0.011478	0.010240	0.011651	0.013620	0.008155	0.017544
Ca	0.033314	0.061909	0.011204	0.013082	0.052694	0.016893
Fe	0.005214	0.008511	0.002580	0.002638	0.007642	0.002808

Table XIV: Estimated Weight Fraction of Asphalt Samples

	ORNL-J1 ±11.98%	ORNL-J2 ±10.15%	ORNL-S1 ±11.02%	ORNL-S2 ±11.01%
H	0.004068	0.033058	0.000005	0.018819
C	0.817196	0.094455	0.999778	0.180038
N	0.000072	0.000367	0.000000	0.000328
O	0.091751	0.465971	0.000111	0.415129
Na	0.002334	0.011866	0.000003	0.010563
Mg	0.004523	0.023391	0.000005	0.020481
Al	0.009259	0.044716	0.000011	0.041807
Si	0.043098	0.185154	0.000053	0.187272
S	0.000523	0.002316	0.000001	0.002291
K	0.003250	0.016204	0.000004	0.014710
Ca	0.017186	0.088484	0.000021	0.077919
Ti	0.000689	0.003535	0.000001	0.003121
V	0.000004	0.000020	0.000000	0.000019
Mn	0.000063	0.000300	0.000000	0.000284
Fe	0.005673	0.027726	0.000007	0.025685
Ni	0.000000	0.000002	0.000000	0.000002
Pb	0.000312	0.002433	0.000000	0.001535

It can be seen that both samples of concrete from the same slab have elemental compositions within two points of each other; however, they are not identical due to the heterogeneous makeup of concrete. Asphalt has results within 10% of each other with the exception of ORNL-S1. This discrepancy would most likely be reduced if percent transmission was calculated at more energy levels. Therefore, the transmission experiment was repeated with an Eu-152 source, yielding the data seen in Table XV. The newly measured transmissions through asphalt were added to the previous rates. This new data set was also fed through the C++ program, which estimated the composition seen in Table XVI. To determine the material source card for MCNP, an average of the asphalt results is taken. This yielded the material card seen in Figure 13.

Table XV: Percent Transmission of Eu-152 through the Four Asphalt Samples

	ORNL-J1	ORNL-J2	ORNL-S1	ORNL-S2
121.78 keV	32.19±0.001	24.70±0.001	22.42±0.001	29.20±0.001
244.69 keV	41.05±0.01	35.44±0.01	32.19±0.01	38.57±0.01
344.27 keV	44.80±0.01	40.32±0.01	35.91±0.004	43.35±0.01
367.79 keV	44.44±0.45	38.89±0.43	32.32±0.38	44.44±0.44
411.11 keV	41.57±0.12	43.70±0.12	40.24±0.11	41.77±0.11
443.98 keV	42.98±0.10	47.75±0.11	36.14±0.08	47.05±0.11
778.89 keV	57.49±0.05	56.31±0.05	51.23±0.04	55.88±0.05
867.32 kev	53.42±0.19	50.27±0.18	46.85±0.17	54.79±0.20
964.01 keV	57.53±0.05	59.22±0.05	53.01±0.04	59.67±0.05
1112.02 keV	64.75±0.07	60.64±0.06	52.94±0.05	58.87±0.06
1407.95 keV	63.98±0.06	62.38±0.05	57.52±0.04	60.97±0.05

Table XVI: New Estimated Weight Fraction of Asphalt Samples

	ORNL-J1 ±7.99%	ORNL-J2 ±29.7%	ORNL-S1 ±21.1%	ORNL-S2 ±6.13%
H	0.044879	0.021927	0.481023	0.009053
C	0.049027	0.041357	0.079857	0.075662
N	0.000573	0.000389	0.000203	0.000373
O	0.697073	0.492833	0.258393	0.469827
Na	0.017799	0.012541	0.006630	0.011938
Mg	0.028147	0.024547	0.014520	0.021868
Al	0.050028	0.049290	0.014795	0.050118
Si	0.051328	0.203932	0.074881	0.236197
S	0.001409	0.002545	0.000944	0.002844
K	0.009270	0.017755	0.007187	0.015719
Ca	0.044294	0.094646	0.049240	0.077628
Ti	0.001870	0.003786	0.001948	0.003141
V	7.45E-06	0.000023	6.32E-06	0.000021
Mn	0.000055	0.000349	0.000089	0.000294
Fe	0.004240	0.031825	0.009585	0.025109
Ni	2.71E-07	2.03E-06	6.10E-07	1.60E-06
Pb	3.11E-07	0.002253	0.000698	0.000205

```
m9      1000  -0.139221
        6000  -0.061476
        7000  -0.000384
        8000  -0.479532
       11000  -0.012227
       12000  -0.022270
       13000  -0.041058
       14000  -0.141584
       16000  -0.001936
       19000  -0.012482
       20000  -0.066452
       22000  -0.002687
       23000  -1.44e-05
       25000  -0.000197
       26000  -0.017690
       28000  -1.13e-06
       82000  -0.000789
```

Figure 13: Calculated MCNP Material Card for Asphalt

IV.C. Comparison of Code Results to NAA

First, the concrete sample compositions found through NAA and that estimated in the previous section are directly compared.23 Table XVII - Table XIX list the compositions. As can be seen, the sample composition determined by both methods for the same sample is varied. While oxygen is the major component in both cases, the other major constituent, silicon, is much lower from densitometry than the NAA measurements; instead, calcium accounts for a higher percentage in densitometry. This discrepancy can be explained because the initial guess, based on the composition of concrete from the PNNL material handbook, used in the densitometry program has greater level of calcium than silicon. However, in the range of interest for gammas, both silicon and calcium have very similar mass attenuation coefficients. The reason no manganese is seen in the densitometry estimation is due to it not being in the initial guess. Another set of elements that show noticeable discrepancy is hydrogen and carbon. In the NAA results, both of these elements were not directly measured. Additionally Ryan et al. showed that changes in concentration of both elements results in changes in count rates; however, these variation are only 1%. As for the remaining elements, they are within 5% of the total. This difference can be explained by the nature of both measurement techniques and the heterogeneity of concrete. In both methods, only a portion of the sample is analyzed rather than the entire sample. This means that there will be variations in sample measurements.

Table XVII: Weight Fractions of Concrete Samples from Slab F

	F1		F2	
	Dens	NAA	Dens	NAA
	±20.62%	±2.46%	±21.18%	±1.59%
H	0.03371	0.005	0.01761	0.005
C	0.00392	0.1629	0.00196	0.1461
O	0.53125	0.4845	0.5495	0.4872
Na	0.01408	0.00026	0.01451	0.00032
Mg	0.0011	0.0119	0.00128	0.0106
Al	0.01712	0.00444	0.02124	0.00624
Si	0.34882	0.0151	0.31324	0.0186
K	0.01148	0.00109	0.01024	0.00168
Ca	0.03331	0.3101	0.06191	0.3188
Mn	N/A	0.0003	N/A	0.00036
Fe	0.00521	0.00437	0.00851	0.00541

Table XVIII: Weight Fractions of Concrete Samples from Slab G

	G1		G2	
	Dens	NAA	Dens	NAA
	±20.18%	±1.02%	±20.22%	±1.53%
H	0.08016	0.005	0.125	0
C	0.00994	0.0233	0.01638	0.0005
O	0.51062	0.4727	0.39963	0.4731
Na	0.0136	0.0187	0.01065	0.02
Mg	0.00089	0.00378	0.00068	0.00359
Al	0.0125	0.0618	0.01018	0.066
Si	0.34686	0.2662	0.40815	0.2952
K	0.01165	0.0266	0.01362	0.0327
Ca	0.0112	0.1006	0.01308	0.0898
Mn	N/A	0.00079	N/A	0.00115
Fe	0.00258	0.0213	0.00264	0.0191

Table XIX: Weight Fractions of Concrete Samples from Slab L

	L1		L2	
	Dens	NAA	Dens	NAA
	±20.22%	±3.14%	±19.62%	±1.28%
H	0.02955	0.005	0.11911	0.005
C	0.00337	0.1429	0.01602	0.1194
O	0.61424	0.4769	0.28352	0.4821
Na	0.01625	0.00073	0.00755	0.00102
Mg	0.00134	0.0109	0.00049	0.0089
Al	0.02163	0.0153	0.00804	0.0174
Si	0.24513	0.0475	0.52803	0.0533
K	0.00816	0.0069	0.01754	0.00771
Ca	0.05269	0.2848	0.01689	0.2946
Mn	N/A	0.00048	N/A	0.0005
Fe	0.00764	0.00909	0.00281	0.00151

Although the measured composition is different between the two methods, it was initially proposed that the actual composition isn't as important as material attenuation. To validate this assumption an MCNP deck, described in Chapter III.H, modeling the transmission experiment with energy bins for the energy region of interest was used to calculate the percent transmission through each sample. The material card for the sample, in the MCNP deck, was set to the composition found through both NAA and densitometry. A comparison of these rates can be seen in Table XX -Table XXII.

Table XX: Calculated vs. Measured Transmission at 88.03 keV for Concrete Samples

Sample	Measured	Densitometry	NAA
F1	34.82±0.01	36.97±0.38	32.90±0.43
F2	32.74±0.01	34.82±0.41	30.59±0.46
G1	31.54±0.01	32.19±0.44	30.66±0.46
G2	32.38±0.01	32.87±0.43	33.31±0.43
L1	34.62±0.01	36.66±0.39	32.53±0.43
L2	35.13±0.01	35.93±0.40	34.96±0.41

Table XXI: Calculated vs. Measured Transmission at 661.66 keV for Concrete Samples

Sample	Measured	Densitometry	NAA
F1	66.44±0.01	62.00±0.26	62.81±0.25
F2	65.31±0.01	60.89±0.26	61.25±0.26
G1	62.00±0.01	57.07±0.27	59.60±0.26
G2	62.68±0.01	58.01±0.27	61.79±0.26
L1	65.28±0.01	61.80±0.26	62.50±0.25
L2	65.93±0.01	61.28±0.26	64.52±0.25

Table XXII: Calculated vs. Measured Transmission at 1332.5 keV for Concrete Samples

Sample	Measured	Densitometry	NAA
F1	73.23±0.01	71.11±0.24	71.83±0.24
F2	72.82±0.01	70.28±0.24	70.52±0.24
G1	69.36±0.01	67.06±0.24	69.02±0.24
G2	70.01±0.01	67.77±0.24	70.90±0.24
L1	73.58±0.01	70.95±0.24	71.56±0.24
L2	71.83±0.01	70.52±0.24	73.09±0.24

The data shows the elemental compositions determined from densitometry and NAA yield simulated percent transmission within 10% of each other. Both are within 20% of the measured values.

IV.D. Model Validation

To confirm the results from the methodology, the updated RPM MCNP deck was ran with the various sources of background radiation. The simulated detector responses using both the NAA and estimated elemental concrete compositions were then compared to these measured count rates in the RPM. The theoretical and measured count rates for collimated and uncollimated detectors with slabs F & G are plotted in Figures 14 and 15. It can be seen that the simulated count rates for both samples from the same source are within 1% of each other. Additionally, it shows that using the elemental composition determined from densitometry yielded results within 5% of the results using the composition from NAA. Comparing the simulated count rate to the measured count rate shows that they are within 10%. This shows that the developed methodology provides an accurate estimation of the count rate in an RPM.

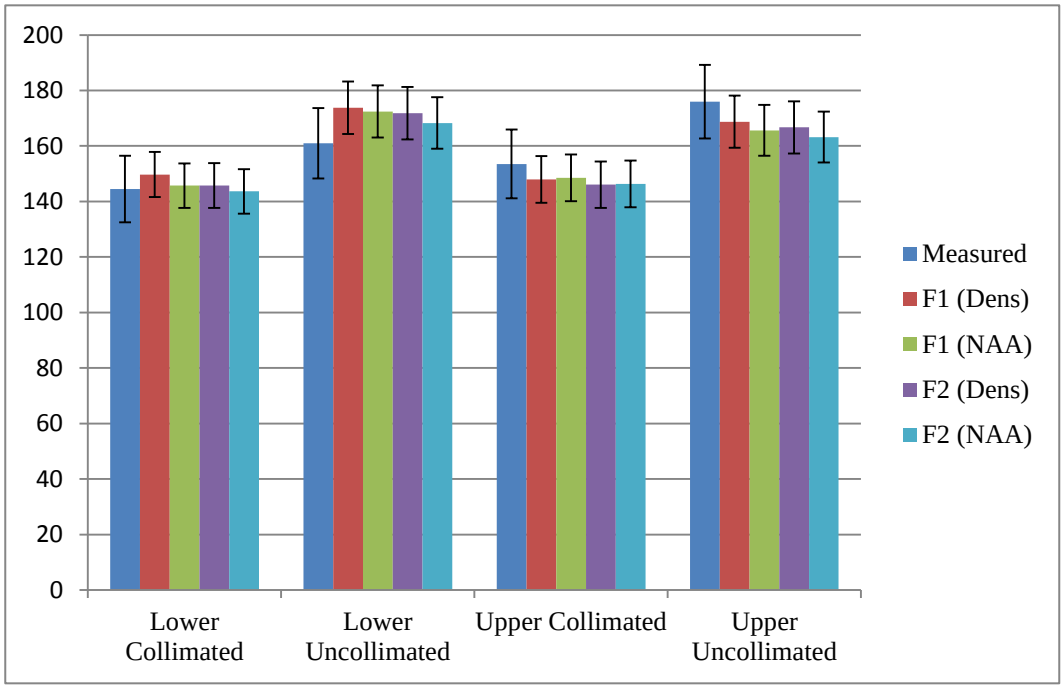

Figure 14: Measured vs. Simulated RPM Count Rates with Slab F Present

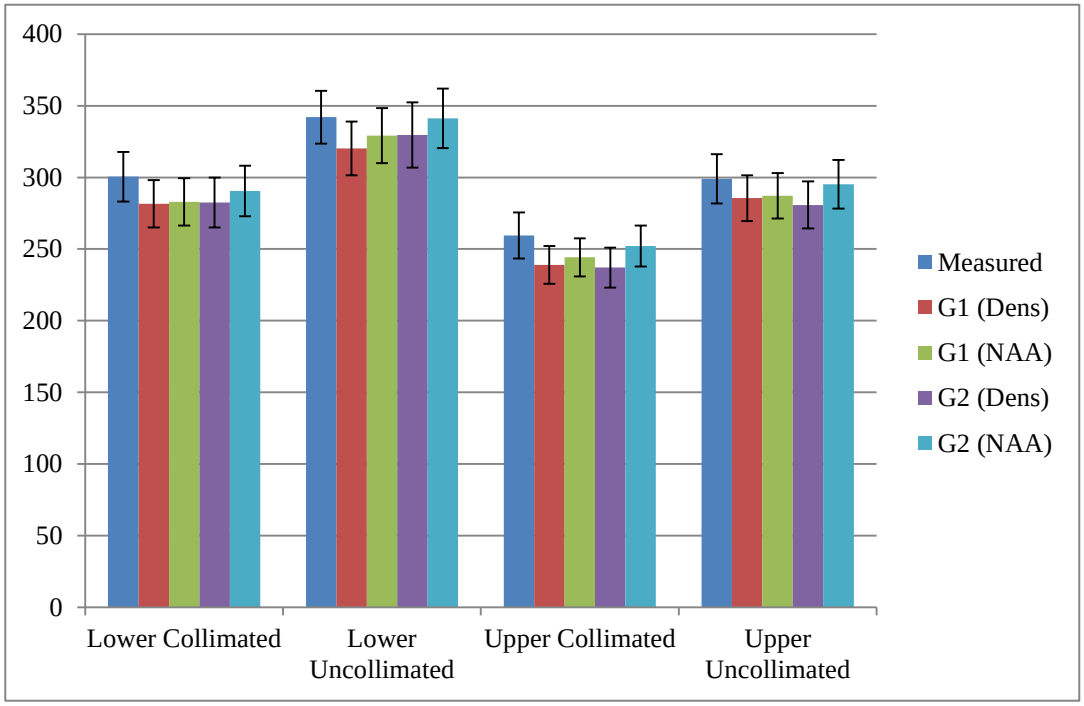

Figure 15: Measured vs. Simulated RPM Count Rates with Slab G Present

CHAPTER V

SUMMARY AND CONCLUSIONS

It is important that RPMs deployed worldwide are able to detect gamma radiation given off by SNM over natural background gamma radiation. This research relied on a combination of direct measurements, a computational equation solver, and photon transport models to provide a methodology for determining the natural gamma ray background at an RPM site.

Samples of asphalt were obtained from ORNL and their activities were determined. Additionally, activity measurements were performed in-situ at ORNL's VM-250AG portal monitor site. Using ISOCS, an efficiency curve was generated for each detector-source configuration. Using GENIE 2000, this data was analyzed providing sample activity, which was turned into an MCNP source card.

Densitometry was also performed on the asphalt samples as well as concrete samples provided by ORNL. The photon transmission through each sample was determined and input into a C++ program to solve the system of densitometry equations. This solution was used to create an MCNP materials card for the samples. The material compositions determined from this method were then compared to results previously obtained from NAA and their percent transmissions were both found to be within 10% of the measured results. Finally, MCNP was used to validate the model and the simulated background counts were compared to measured results.

It was shown that an in-situ count is necessary to accurately determine specific activity and assuming the chain is in secular equilibrium is not valid. Additionally, densitometry was shown to provide an accurate estimation of elemental composition. When the estimated composition from densitometry is compared against the composition found through NAA, it shows that they provide similar results. This is very beneficial as it takes much less time and equipment to determine the percent transmission of the samples. The final implementation of the methodology is as follows:

1. Take in-situ measurement at site
2. Obtain samples
3. Develop ISOCS model
4. Create MCNP source card
5. Measure sample physical properties
6. Determine transmission rate of known energy gammas (Cd-109, Cs-137, Co-60, Eu-152, etc.)
7. Input transmission rates and physical properties into C++ program
8. Create MCNP material card
9. Run MCNP model
10. Determine if physical mitigation methods are needed

REFERENCES

1. National Nuclear Security Administration, "Fact Sheet: NNSA's Second Line of Defense Program." February 1, 2011. https://nnsa.energy.gov/mediaroom/factsheets/nnsassecondlineofdefenseprogram (accessed March 9, 2012).

2. Canberra Industries, "In Situ Gamma Spectroscopy with ISOCS, an In Situ Object Counting System," Document M2352, November 2008. http://www.canberra.com/pdf/Literature/M2352-InSitu-ISOCS-AN.pdf (accessed March 9, 2012).

3. D A SHEA, U.S. Congressional Research Service, "The Global Nuclear Detection Architecture: Issues for Congress" RL34574, July 16, 2008. http://www.fas.org/sgp/crs/nuke/RL34564.pdf (accessed March 9, 2012).

4. R C RUNKLE, L E SMITH, and A J PEURRUNG, "The photon haystack and emerging radiation detection technology," *J. Appl. Phys.* 106, 041101, 2009. doi: 10.1063/1.3207769.

5. R D EVANS, *The Atomic Nucleus*, McGraw-Hill; reprinted 1982, R E Krieger, Malabar, FL 1955.

6. R YORK, "Portal Monitor Fundamentals," Oak Ridge National Laboratory, Oak Ridge TN, 10-11 August 2010. Conference Presentation Handout.

7. TSA Systems, Ltd., "Vehicle and Pedestrian Monitor: VM-250AGN / VM-700AGN, Operations & Service Manual," Document #5000, Revision A, January 2006.

8. L A CURRIE, "Limits for Qualitative Detection and Quantitative Determination: Application to Radiochemistry," *Anal. Chem.* 40, 3, 586-93, 1968.

9. C M LEDERER, V S SHIRLEY, E BROWNE, J M DAIRIKI, R E DOEBLER, et. al., *Table of Isotopes*, 7th Edition, John Wiley & Sons, New York City, NY, 1977.

10. R TRKVA and D BERG, *Man-Made and Natural Radioactivity in Environmental Pollution and Radiochronology*, Kluwer Academic Publishers, Dordrecht The Netherlands, 2004.

11. S M ROBINSON, W R KAYE, J E SCHWEPPE, and E R SICILIANO, "Optimal Background Attenuation for Fielded Radiation Detection Systems," *IEEE Transactions on Nuclear Science*, 54, 4, 1279-84, August 2007.

12. J ELY, R KOUZES, J SCHWEPPE, E SICILIANO, D STRACHAN, and D WEIER, "The use of energy windowing to discriminate SNM from NORM in radiation portal monitors," *Nuclear Instruments and Methods in Physics Research A*, 560, 373–87, 2006.

13. Canberra Industries, Inc., "Genie™ 2000 Spectroscopy Software: Operations," Version 3.2, Canberra Industries, Meridian CT, 2009.

14. Canberra Industries, Inc., "Genie™ 2000 Spectroscopy Software: Customization Tools," Version 3.2, Canberra Industries, Meridian, CT, 2009.

15. G GILMORE, *Practical Gamma-Ray Spectrometry*, 2nd Edition, John Wiley & Sons Ltd., West Sussex UK, 2008.

16. R VENKATARAMAN, F BRONSON, V ALRASHKEVICH, B M YOUNG, and M. FIELD, "Validation of in situ Object Counting System (ISOCS) Mathematical Efficiency Calibration Software," *Nucl. Instrum. Meth. A.* 422, 450-454, 1999.

17. A A BOL'SHAKOV, A A GANEE, and V M NEMETS, "Prospects in analytical Atomic Spectrometry," *Russian Chemical Reviews* 75, 4, 289-302, 2006.

18. D REILLY, N ENSSLIN, H SMITH JR, and S KREINER, *Passive Nondestructive Assay of Nuclear Materials*, U.S. Nuclear Regulatory Commission, Washington DC, 1991.

19. MCNP X-5 Monte Carlo Team, "MCNP—A General Purpose Monte Carlo NParticle Transport Code, Version 5," LA UR 03 1987, Los Alamos National Laboratory, April 2003.

20. Canberra Industries, "Model S573 ISOCS Calibration Software: Technical Reference Manual," Version 4.2, Meridian CT, 2009.

21. R G WILLIAMS III, C J GESH, and R T PAGH, "Compendium of Material Composition Data for Radiation Transport Modeling," PNNL-15870, Pacific Northwest National Laboratory, Richland WA, April 2006.

22. W N MCELROY, S BERG, T CROCKETT, and R HAWKINS, "A Computer-Automated Iterative Method for Neutron Flux Spectral Determination by Foil Activation," AFWL-TR-67-41, Vol. 1, Air Force Weapons Laboratory, Kirkland NM, July 1967.

23. C M RYAN, *Determining the Impact of Concrete Roadways on Gamma Ray Background Readings for Radiation Portal Monitoring Systems*, MS Thesis, Texas A&M University, College Station TX, 2011. Print.

APPENDIX A

HPGe gamma ray spectra

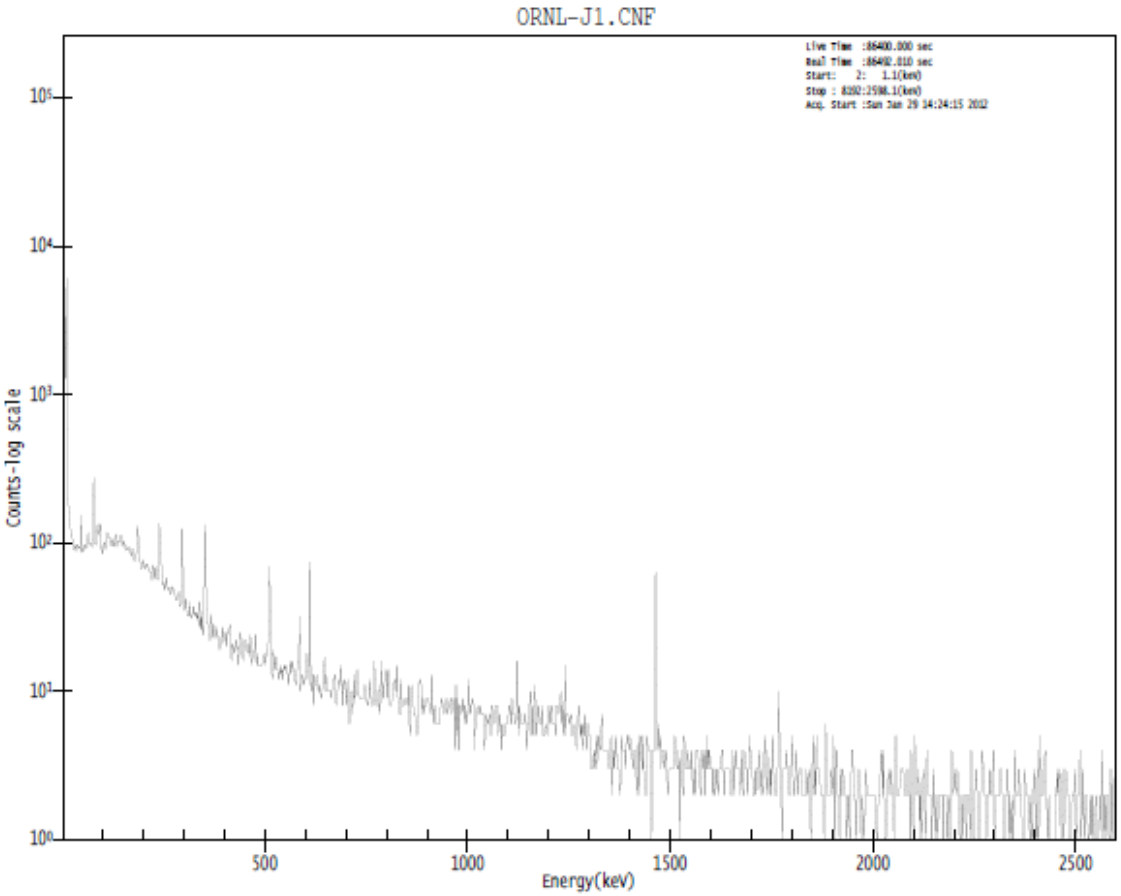

Figure A.1. HPGe gamma spectrum from sample J1.

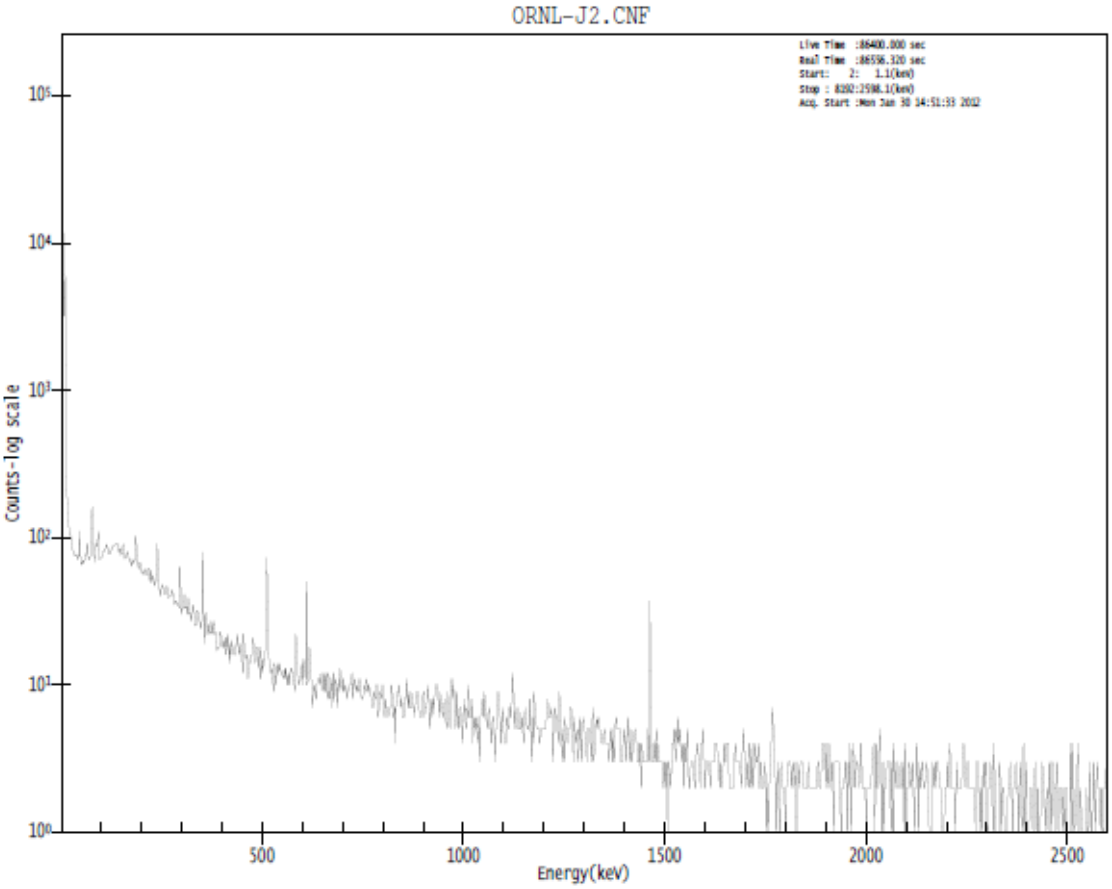

Figure A.2. HPGe gamma spectrum from sample J2.

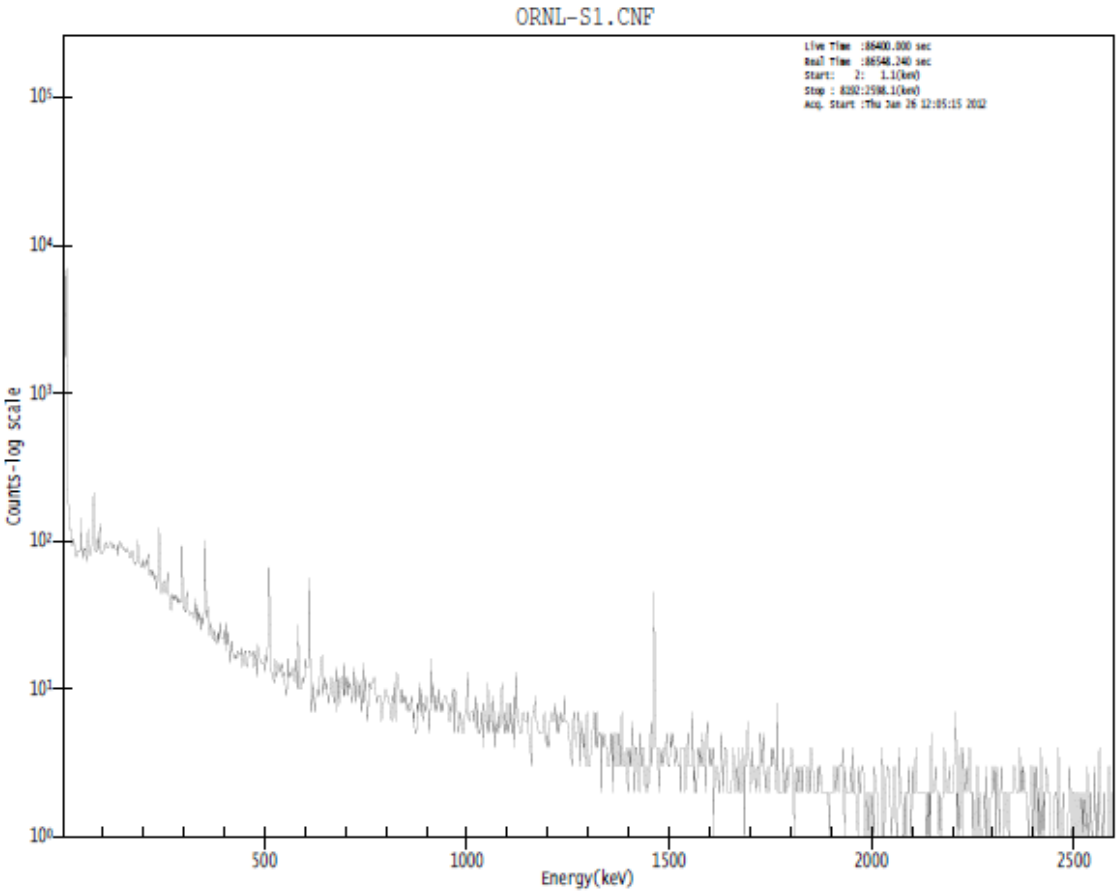

Figure A.3. HPGe gamma spectrum from sample S1.

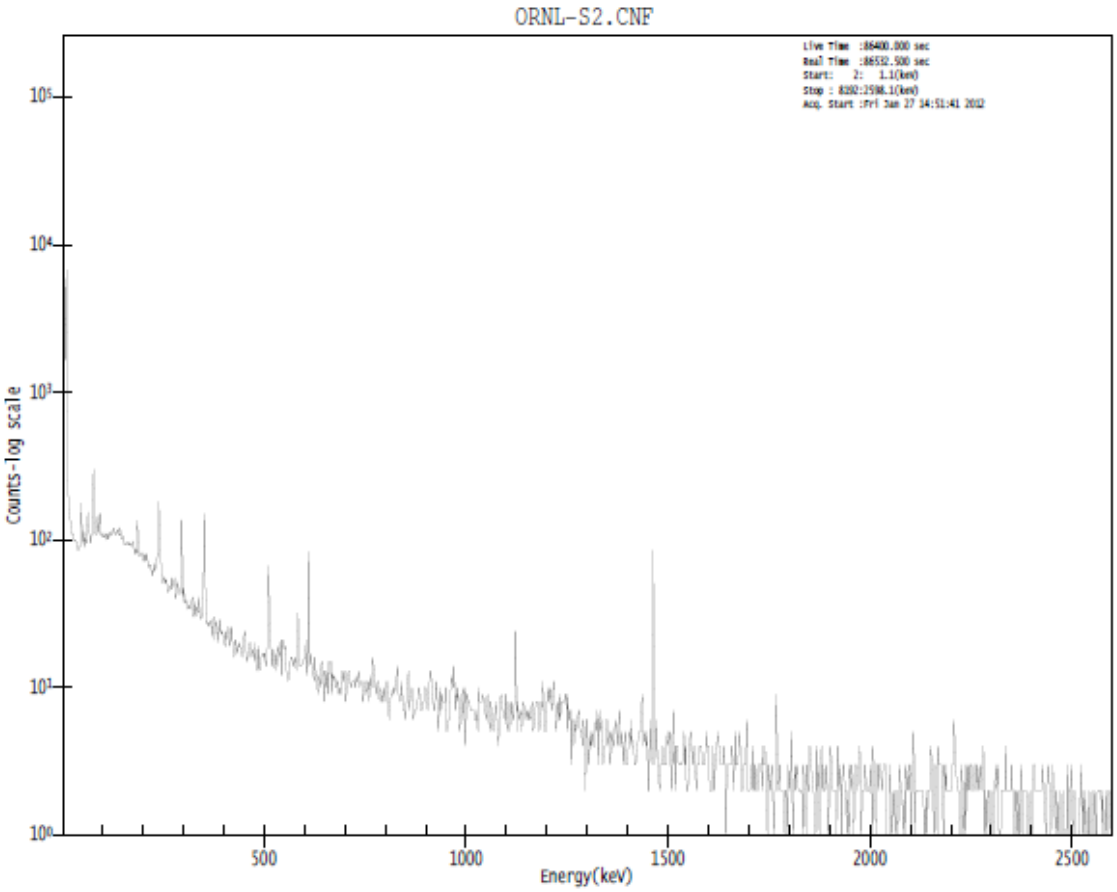

Figure A.4. HPGe gamma spectrum from sample S2.

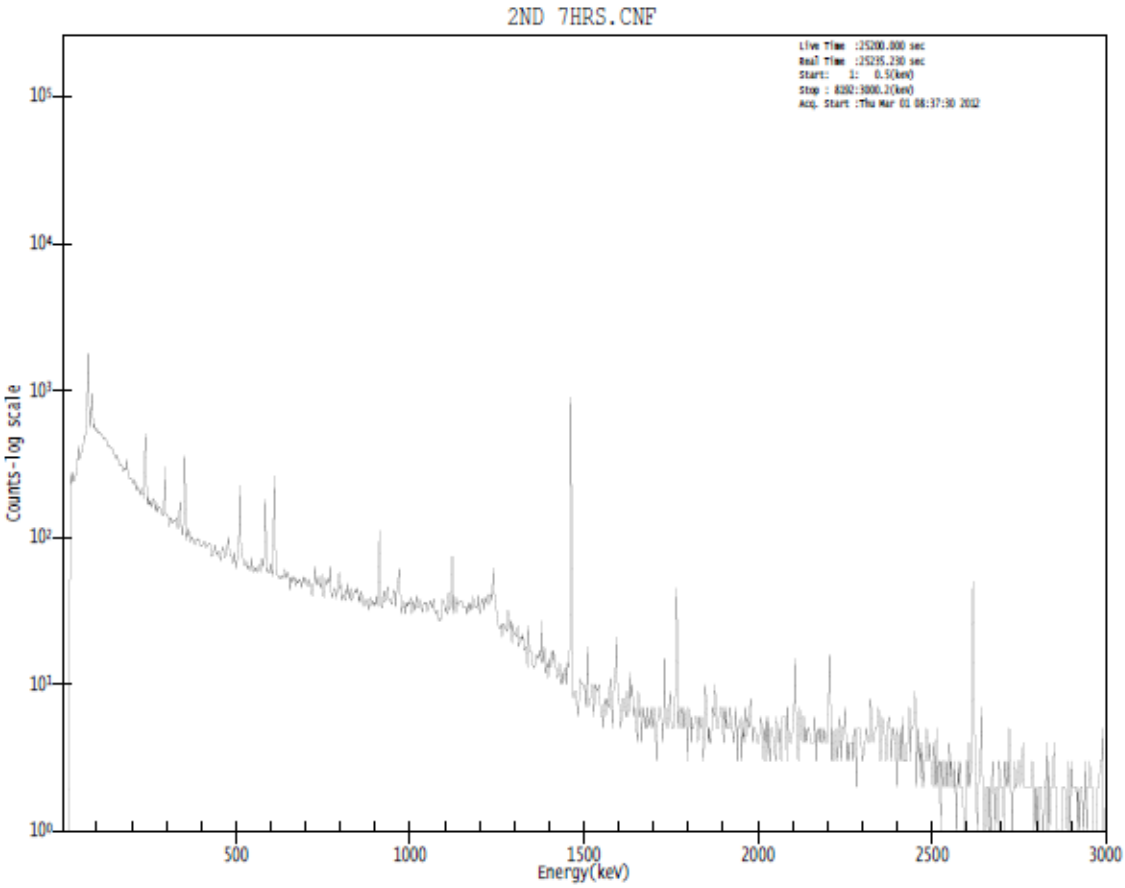

Figure A.5. HPGe gamma spectrum from the in-situ count.

APPENDIX B

ISOCS™ Efficiency Calibration Input Parameters

Table B.1. ISOCS™ Efficiency Calibration Input Parameters for Asphalt Sample S1

No.	Dimensions (cm)					Material	Density	Rel.
	d.1	d.2	d.3	d.4	d.5		(g cm-3)	Conc.
1	0.00001	10.287	9.6266	3.302	N/A	asphalt	1.64	N/A
2	9.6266	N/A	N/A	N/A	N/A	asphalt	1.64	1
3	0	N/A	N/A	N/A	N/A	asphalt	1.64	0
4	0	N/A	N/A	N/A	N/A	(none)	0	N/A
5	0	N/A	N/A	N/A	N/A	(none)	0	N/A
6	8.50	0	0	0	0	N/A	N/A	N/A

Table B.2. ISOCS™ Efficiency Calibration Input Parameters for Asphalt Sample S2

No.	Dimensions (cm)					Material	Density	Rel.
	d.1	d.2	d.3	d.4	d.5		(g cm-3)	Conc.
1	0.00001	11.918	11.572	4.572	N/A	asphalt	1.743	N/A
2	11.572	N/A	N/A	N/A	N/A	asphalt	1.743	1
3	0	N/A	N/A	N/A	N/A	asphalt	1.743	0
4	0	N/A	N/A	N/A	N/A	(none)	0	N/A
5	0	N/A	N/A	N/A	N/A	(none)	0	N/A
6	8.5	0	0	0	0	N/A	N/A	N/A

Table B.3. ISOCS™ Efficiency Calibration Input Parameters for Asphalt Sample J1

No.	Dimensions (cm)					Material	Density (g cm-3)	Rel. Conc.
	d.1	d.2	d.3	d.4	d.5			
1	1E-05	10.6	11.2	4.57	N/A	asphalt	1.633	N/A
2	11.201	N/A	N/A	N/A	N/A	asphalt	1.633	1
3	0	N/A	N/A	N/A	N/A	asphalt	1.633	0
4	0	N/A	N/A	N/A	N/A	(none)	0	N/A
5	0	N/A	N/A	N/A	N/A	(none)	0	N/A
6	8.50	0	0	0	0	N/A	N/A	N/A

Table B.4. ISOCS™ Efficiency Calibration Input Parameters for Asphalt Sample J2

No.	Dimensions (cm)					Material	Density (g cm-3)	Rel. Conc.
	d.1	d.2	d.3	d.4	d.5			
1	0.00001	8.175	7.3546	4.013	N/A	asphalt	1.49	N/A
2	7.3546	N/A	N/A	N/A	N/A	asphalt	1.49	1
3	0	N/A	N/A	N/A	N/A	asphalt	1.49	0
4	0	N/A	N/A	N/A	N/A	(none)	0	N/A
5	0	N/A	N/A	N/A	N/A	(none)	0	N/A
6	8.50	0	0	0	0	N/A	N/A	N/A

Table B.5. ISOCS™ Efficiency Calibration Input Parameters for in-situ Asphalt

No.	Dimensions (cm)					Material	Density (g cm-3)	Rel. Conc.
	d.1	d.2	d.3	d.4	d.5			
1		2000	2000	N/A	N/A	asphalt	1.72	N/A
2	5	N/A	N/A	N/A	N/A	asphalt	1.72	0.5
3	10	N/A	N/A	N/A	N/A	rock	2.662	0.5
4	2000	N/A	N/A	N/A	N/A	earth	1.52	0
5	0	N/A	N/A	N/A	N/A	(none)	0	0
6	0	N/A	N/A	N/A	N/A	(none)	0	0
7	0	N/A	N/A	N/A	N/A	(none)	0	0
8	0	N/A	N/A	N/A	N/A	(none)	0	0
9	0	N/A	N/A	N/A	N/A	(none)	0	0
10	0	N/A	N/A	N/A	N/A	(none)	0	0
11	0	N/A	N/A	N/A	N/A	(none)	0	0
12	0	N/A	N/A	N/A	N/A	(none)	0	N/A
13	0	N/A	N/A	N/A	N/A	(none)	0	N/A
14	73.342	0	0	0	0	N/A	N/A	N/A

APPENDIX C

MCNP input deck for VM-250AG RPM setup at ORNL

```
Portal Monitor Environmental Gamma Background Study
c Created by Alexander Solodov, GNSTD, Oak Ridge National Laboratory
c Modified by Christopher Ryan, NSSPI, Texas A&M University
c Modified by Nandan G. Chandregowda, NSSPI, Texas A&M University
c Modified by Matthew Fitzmaurice, NSSPI, Texas A&M University
c   Asphalt + Concrete
c -------------------------------CELL CARDS-------------------------------------
c 1  1  -2.301    -100          imp:p=1 $ F1 Concrete Slab "layer 1"
c 2  1  -2.301    -101          imp:p=2 $ F1 Concrete Slab "layer 2"
c 3  1  -2.301    -102          imp:p=4 $ F1 Concrete Slab "layer 3"
6  9  -2.301    -106          imp:p=1 $ asphalt around RPM
9  2  -2.700    -109          imp:p=4 $ Aluminum (Right Portal, Front)
10 5  -7.920    -110 +111       imp:p=4 $ SS304 (Right Portal, Back & Sides)
11 4  -1.032    -112          imp:p=4 $ PVT (Right Lower Detector)
12 4  -1.032    -113          imp:p=4 $ PVT (Right Upper Detector)
13 3  -1.205E-3 -111 +112 +113 +114 +115 #34 #35 #36 #37 #38
       #39 #40 #41 #42 #43 #44 #45 #46 #47 #48 #49 #50 #51
       #52 #53 #54 #55 #56 #57 #58 #59 #60 #61 imp:p=4 $ Interior Air (Right Portal
Arm)
14 6  -11.34    -114 +112 +116  imp:p=4 $ Shielding, Lead (Right Lower Detector)
15 6  -11.34    -115 +113 +117  imp:p=4 $ Shielding, Lead (Right Upper Detector)
16 7  -1.19     -116          imp:p=4 $ PMMA (Right Lower Detector)
17 7  -1.19     -117          imp:p=4 $ PMMA (Right Upper Detector)
19 2  -2.700    -119          imp:p=4 $ Aluminum (Left Portal, Front)
20 5  -7.920    -120 +121       imp:p=4 $ SS304 (Left Portal, Back & Sides)
21 4  -1.032    -122          imp:p=4 $ PVT (Left Lower Detector)
22 4  -1.032    -123          imp:p=4 $ PVT (Left Upper Detector)
23 3  -1.205E-3 -121 +122 +123 +124 +125 +128 +130 #28 #29 #62
       #63 #64 #65 #66 #67 #68 #69 #70 #71 #72 #73 #74 #75
       #76 #77 #78 #79 #80 #81 #82 #83 #84 #85 #86 #87 #88 #89 imp:p=4 $ Interior
Air (Left Portal Arm)
24 6  -11.34    -124 +122 +126  imp:p=4 $ Shielding, Lead (Left Lower Detector)
25 6  -11.34    -125 +123 +127  imp:p=4 $ Shielding, Lead (Left Upper Detector)
26 7  -1.19     -126          imp:p=4 $ PMMA (Left Lower Detector)
27 7  -1.19     -127          imp:p=4 $ PMMA (Left Upper Detector)
c ---------------------------Collimators-----------------------------------------
28 8  -7.820    -128 #4       imp:p=4 $ left lower collimator
4  3  -1.205E-3 -129          imp:p=4
29 8  -7.820    -130 #5       imp:p=4 $ left upper collimator
```

```
5  3  -1.205E-3 -131          imp:p=4
c --------------------------Steel plates---------------------------------------
30 8  -7.820    -132          imp:p=4 $ right portal steel plate 1
31 8  -7.820    -133          imp:p=4 $ right portal steel plate 2
32 8  -7.820    -134          imp:p=4 $ left portal steel plate 3
33 8  -7.820    -135          imp:p=4 $ left portal steel plate 4
c Electronics in Right Portal
34 2  -2.700      -136          imp:p=4 $ Plate
35 10 -1.5370     -137            imp:p=4 $ A Right
36 10 -1.5370     -138            imp:p=4 $ B Right
37 10 -1.5370     -139            imp:p=4 $ C Right
38 10 -1.5370     -140            imp:p=4 $ D Right
39 10 -1.5370     -141            imp:p=4 $ E Right
40 10 -1.5370     -142   #39      imp:p=4 $ F Right
41 10 -1.5370     -143            imp:p=4 $ G Right
42 10 -1.5370     -144   #41      imp:p=4 $ H Right
43 10 -1.5370     -145            imp:p=4 $ I Right
44 10 -1.5370     -146   #43      imp:p=4 $ J Right
45 2  -2.700      -147          imp:p=4 $ K- Thin Plate
46 10 -1.5370     -148            imp:p=4 $ L Right
47 10 -1.5370     -149            imp:p=4 $ M Right
48 10 -1.5370     -150            imp:p=4 $ N Right
49 10 -1.5370     -151   #48      imp:p=4 $ O Right
c  Right Lower Neutron Detector
50 11 -0.92 -152 #51 (154:-158:159) (155:-160:161)
                (156:-158:159) (157:-160:161) imp:p=4 $ Poly - Outer Surface
51 3 -1.205E-3 -153  (154:-158:159) (155:-160:161)
                (156:-158:159) (157:-160:161) imp:p=4 $ Poly - Inner Surface
52 12 -8.03 -154 158 -159  (155:-160:161)       imp:p=4 $ He3-1- Outer Wall
53 13 -0.0007144 -155 160 -161                  imp:p=4 $ He3-1
54 12 -8.03 -156 158 -159  (157:-160:161)       imp:p=4 $ He3-2- Outer Wall
55 13 -0.0007144 -157 160 -161                  imp:p=4 $ He3-2
c  Right Upper Neutron Detector
56 11 -0.92 -162 #57 (164:-168:169) (165:-170:171)
                (166:-168:169) (167:-170:171) imp:p=4 $ Poly - Outer Surface
57 3 -1.205E-3 -163  (164:-168:169) (165:-170:171)
                (166:-168:169) (167:-170:171) imp:p=4 $ Poly - Inner Surface
58 12 -8.03 -164 168 -169  (165:-170:171)       imp:p=4 $ He3-1- Outer Wall
59 13 -0.0007144 -165 170 -171                  imp:p=4 $ He3-1
60 12 -8.03 -166 168 -169  (167:-170:171)       imp:p=4 $ He3-2- Outer Wall
61 13 -0.0007144 -167 170 -171                  imp:p=4 $ He3-2
c Electronics in left portal
62 2  -2.700      -180          imp:p=4 $ Plate Left
63 10 -1.5370     -181            imp:p=4 $ A Left
```

```
64 10 -1.5370     -182          imp:p=4 $ B Left
65 10 -1.5370     -183          imp:p=4 $ C Left
66 10 -1.5370     -184          imp:p=4 $ D Left
67 10 -1.5370     -185          imp:p=4 $ E Left
68 10 -1.5370     -186  #67     imp:p=4 $ F Left
69 10 -1.5370     -187          imp:p=4 $ G Left
70 10 -1.5370     -188  #69     imp:p=4 $ H Left
71 10 -1.5370     -189          imp:p=4 $ I Left
72 10 -1.5370     -190  #71     imp:p=4 $ J Left
73 2  -2.700      -191          imp:p=4 $ K- Thin Plate Left
74 10 -1.5370     -192          imp:p=4 $ L Left
75 10 -1.5370     -193          imp:p=4 $ M Left
76 10 -1.5370     -194          imp:p=4 $ N Left
77 10 -1.5370     -195  #76     imp:p=4 $ O Left
c  Left Lower Neutron Detector
78 11 -0.92 -196 #79 (198:-202:203) (199:-204:205)
                (200:-202:203) (201:-204:205) imp:p=4 $ Poly - Outer Surface
79 3 -1.205E-3 -197  (198:-202:203) (199:-204:205)
                (200:-202:203) (201:-204:205) imp:p=4 $ Poly - Inner Surface
80 12 -8.03 -198 202 -203  (199:-204:205)       imp:p=4 $ He3-1- Outer Wall
81 13 -0.0007144 -199 204 -205                  imp:p=4 $ He3-1
82 12 -8.03 -200 202 -203  (201:-204:205)       imp:p=4 $ He3-2- Outer Wall
83 13 -0.0007144 -201 204 -205                  imp:p=4 $ He3-2
c  Left Upper Neutron Detector
84 11 -0.92 -206 #85 (208:-212:213) (209:-214:215)
                (210:-212:213) (211:-214:215) imp:p=4 $ Poly - Outer Surface
85 3 -1.205E-3 -207  (208:-212:213) (209:-214:215)
                (210:-212:213) (211:-214:215) imp:p=4 $ Poly - Inner Surface
86 12 -8.03 -208 212 -213  (209:-214:215)       imp:p=4 $ He3-1- Outer Wall
87 13 -0.0007144 -209 214 -215                  imp:p=4 $ He3-1
88 12 -8.03 -210 212 -213  (211:-214:215)       imp:p=4 $ He3-2- Outer Wall
89 13 -0.0007144 -211 214 -215                  imp:p=4 $ He3-2
c ----------Lower semisphere where particles are killed----------
90 0  -900                  imp:p=0 $ kill particle moving below asphalt
c 91  3 -1.205E-3 +91 -92 #90    imp:p=4
c 92  3 -1.205E-3 +92 -93 #90    imp:p=4
c 93  3 -1.205E-3 +93 -94 #90    imp:p=4
c 94  3 -1.205E-3 +94 -95 #90    imp:p=4
c 95  3 -1.205E-3 +95 -96 #90    imp:p=4
c 96  3 -1.205E-3 +96 -97 #90    imp:p=4
c 97  3 -1.205E-3 +97 -98 #90    imp:p=4
c 98  3 -1.205E-3 +98 -99 #90    imp:p=4
900  3 -1.205E-3 903 -901 905 -904 900 -906
c        #1 #2 #3
```

```
       #6 #32 #33 (306:-307:-302:303:-304:305) imp:p=4
901  3 -1.205E-3 901 -902 905 -904 900 -906
c        #1 #2 #3
       #6 #30 #31 (-300:301:-302:303:-304:305) imp:p=4
903  3 -1.205E-3  -99 +900   (-903:901:-905:904:-900:906)
c        #1 #2 #3
       #6 #30 #31 #32 #33 (-901:902:-905:904:-900:906) imp:p=4
904  0  +99 #90 imp:p=0                    $ The edge of the universe...

c ------------------------------------SURFACE CARDS-----------------------------------------
---
c ---------------------------------Concrete and asphalt-----------------------------------
100 RPP -198.0000  198.0000 -228.250  228.250 -30.480  -20.4800  $ concrete slab
"layer 1"
101 RPP -198.0000  198.0000 -228.250  228.250 -20.480  -10.4800  $ concrete slab
"layer 2"
102 RPP -198.0000  198.0000 -228.250  228.250 -10.480    0.0000  $ concrete slab
"layer 3"
106 RPP -3700.00  3700.00 -3700.0  3700.0 -35.480  -30.4800  $ asphalt
c ------------------------------------Portal Monitor-----------------------------------------
109 RPP  254.0000  254.3175 -33.0000  33.0000 0.00000  304.0000  $ right portal front
face
110 RPP  254.3175  277.0000 -33.0000  33.0000 0.00000  304.0000  $ right portal outer
surf
111 RPP  254.3175  276.6830 -32.6825  32.6825 0.31750  303.6825  $ right portal inner
surf
112 RPP  269.5000  273.5000 -24.5000 -9.50000 23.0000   99.0000  $ right lower
detector surf
113 RPP  269.5000  273.5000 -24.5000 -9.50000 214.000  290.0000  $ right upper
detector surf
114 RPP  269.5000  274.4530 -25.4525 -8.54750 22.0475  112.0000  $ lead around right
lower det surf
115 RPP  269.5000  274.4530 -25.4525 -8.54750 201.000  290.9525  $ lead around right
upper det surf
116 RPP  269.5000  273.5000 -24.5000 -9.50000 99.0000  112.0000  $ lucite right lower
117 RPP  269.5000  273.5000 -24.5000 -9.50000 201.000  214.0000  $ lucite right upper
119 RPP -254.3175 -254.0000 -33.0000  33.0000 0.00000  304.0000  $ left portal front
face
120 RPP -277.0000 -254.3175 -33.0000  33.0000 0.00000  304.0000  $ left portal outer
surf
121 RPP -276.6830 -254.3175 -32.6825  32.6825 0.31750  303.6825  $ left portal inner
surf
122 RPP -273.5000 -269.5000 -24.5000 -9.50000 23.0000   99.0000  $ left lower
detector surf
```

```
123 RPP -273.5000 -269.5000 -24.5000 -9.50000 214.000  290.0000  $ left upper
detector surf
124 RPP -274.4530 -269.5000 -25.4525 -8.54750 22.0475  112.0000  $ lead around left
lower det surf
125 RPP -274.4530 -269.5000 -25.4525 -8.54750 201.000  290.9525  $ lead around left
upper det surf
126 RPP -273.5000 -269.5000 -24.5000 -9.50000 99.0000  112.0000  $ lucite left lower
127 RPP -273.5000 -269.5000 -24.5000 -9.50000 201.000  214.0000  $ lucite left upper
c ---------------------------------------Collimator---------------------------------------------
128 RPP -269.5000 -259.3000 -26.6500 -7.35000 22.0475  105.5475  $ left lower
collimator outer surf
129 RPP -269.5000 -259.3000 -25.7000 -8.30000 22.9975  104.5975  $ left lower
collimator inner surf
130 RPP -269.5000 -259.3000 -26.6500 -7.35000 207.4525 290.9525  $ left upper
collimator outer surf
131 RPP -269.5000 -259.3000 -25.7000 -8.30000 208.4025 290.0025  $ left upper
collimator inner surf
c ---------------------------------------Steel Plates-------------------------------------------
132 RPP  274.5000  277.0000  33.0000  154.000 0.00000  304.0000  $ right portal steel
plate 1
133 RPP  274.5000  277.0000 -154.000  -33.000 0.00000  304.0000  $ right portal steel
plate 2
134 RPP -277.0000 -274.5000  33.0000  154.000 0.00000  304.0000  $ left portal steel
plate 1
135 RPP -277.0000 -274.5000 -154.000  -33.000 0.00000  304.0000  $ left portal steel
plate 2
c  Electronics RIGHT
136 RPP  273.60  273.70  -7.3875   30.1425   121.84  196.465   $ thin plate A
137 RPP  264.39  273.60  14.2625   30.1425   153.60  177.73    $ A Right
138 RPP  264.39  273.60  -4.7875   11.4025   144.07  168.20    $ B Right
139 RPP  264.39  273.60  14.2725   25.8125   125.34  137.09    $ C Right
140 RPP  264.39  273.60  -3.0575    5.6025   188.97  194.74    $ D Right
141 RPP  264.39  273.60  -3.0575    5.6025   183.475 188.525   $ E Right
142 RPP  267.39  273.60  -5.9475    8.4925   184.50  187.40    $ F Right
143 RPP  264.39  273.60  -3.0575    2.5725   176.975 182.025   $ G Right
144 RPP  267.39  273.60  -5.9475    4.8825   178.0   180.9     $ H Right
145 RPP  264.39  273.60  -2.3375    8.4925   119.23  124.28    $ I Right
146 RPP  267.39  273.60  -4.5075   10.4325   120.65  123.155   $ J Right
147 RPP  273.60  273.70  -23.79    -7.91     147.365 183.465   $ K- Thin plate
148 RPP  264.39  273.60  -22.35   -15.13     176.25  182.025   $ L Right
149 RPP  264.39  273.60  -20.52   -13.309    166.9   174.8     $ M Right
150 RPP  264.39  273.60  -12.86   -11.421    168.31  172.64    $ N Right
151 RPP  267.39  273.60  -13.309  -10.972    169.40  171.50    $ O Right
c Right lower neutron detector
```

```
152 RPP  260.80  273.50    2.2     30.14     14.21   112.00    $ Poly - Outer surface
153 RPP  261.80  272.50    3.2     29.14     15.48   110.73    $ Poly - Inner surface
154 C/Z  267.15  9.82  2.50   $ He3 - 1
155 C/Z  267.15  9.82  2.45   $ He3 - 1
156 C/Z  267.15  22.52  2.50  $ He3 - 2
157 C/Z  267.15  22.52  2.45  $ He3 - 2
158 PZ   19.73
159 PZ  110.73
160 PZ   19.93
161 PZ  110.53
c Right Upper neutron detector
162 RPP  260.80  273.50    2.2     30.14    198.21   296.00    $ Poly - Outer surface
163 RPP  261.80  272.50    3.2     29.14    199.48   294.73    $ Poly - Inner surface
164 C/Z  267.15  9.82  2.50   $ He3 - 1
165 C/Z  267.15  9.82  2.45   $ He3 - 1
166 C/Z  267.15  22.52  2.50  $ He3 - 2
167 C/Z  267.15  22.52  2.45  $ He3 - 2
168 PZ  199.48
169 PZ  290.48
170 PZ  199.68
171 PZ  290.28
c  Electronics Left
180 RPP  -273.60  -273.50  -7.3875   30.1425   121.84  196.465   $ thin plate A Left
181 RPP  -273.50  -264.29  14.2625   30.1425   153.60  177.73    $ A Left
182 RPP  -273.50  -264.29  -4.7875   11.4025   144.07  168.20    $ B Left
183 RPP  -273.50  -264.29  14.2725   25.8125   125.34  137.09    $ C Left
184 RPP  -273.50  -264.29  -3.0575    5.6025   188.97  194.74    $ D Left
185 RPP  -273.50  -264.29  -3.0575    5.6025   183.475 188.525   $ E Left
186 RPP  -273.50  -267.29  -5.9475    8.4925   184.50  187.40    $ F Left
187 RPP  -273.50  -264.29  -3.0575    2.5725   176.975 182.025   $ G Left
188 RPP  -273.50  -267.29  -5.9475    4.8825   178.0   180.9     $ H Left
189 RPP  -273.50  -264.29  -2.3375    8.4925   119.23  124.28    $ I Left
190 RPP  -273.50  -267.29  -4.5075   10.4325   120.65  123.155   $ J Left
191 RPP  -273.60  -273.50  -23.79    -7.91     147.365 183.465   $ K- Thin plate
192 RPP  -273.50  -264.29  -22.35   -15.13     176.25  182.025   $ L Left
193 RPP  -273.50  -264.29  -20.52   -13.309    166.9   174.8     $ M Left
194 RPP  -273.50  -264.29  -12.86   -11.421    168.31  172.64    $ N Left
195 RPP  -273.50  -267.29  -13.309  -10.972    169.40  171.50    $ O Left
c Left lower neutron detector
196 RPP  -273.50  -260.80    2.2     30.14     14.21   112.00    $ Poly - Outer surface
197 RPP  -272.50  -261.80    3.2     29.14     15.48   110.73    $ Poly - Inner surface
198 C/Z  -267.15  9.82  3.81   $ He3 - 1
199 C/Z  -267.15  9.82  3.61   $ He3 - 1
200 C/Z  -267.15  22.52  3.81  $ He3 - 2
```

```
201 C/Z  -267.15  22.52  3.61  $ He3 - 2
202 PZ   19.73
203 PZ  110.73
204 PZ   19.93
205 PZ  110.53
c Left Upper neutron detector
206 RPP  -273.50  -260.80    2.2     30.14    198.21   296.00    $ Poly - Outer surface
207 RPP  -272.50  -261.80    3.2     29.14    199.48   294.73    $ Poly - Inner surface
208 C/Z  -267.15  9.82  3.81   $ He3 - 1
209 C/Z  -267.15  9.82  3.61   $ He3 - 1
210 C/Z  -267.15  22.52  3.81  $ He3 - 2
211 C/Z  -267.15  22.52  3.61  $ He3 - 2
212 PZ  199.48
213 PZ  290.48
214 PZ  199.68
215 PZ  290.28
c
300 PX 254.0
301 PX 277.0
302 PY -33.0
303 PY  33.0
304 PZ   0.0
305 PZ 304.0
c
306 PX -254.0
307 PX -277.0
c -------------------------Plane below asphalt to kill particles---------------------------------
900 pz -35.480
901 px 0.0
902 px 400
903 px -400
904 py 100
905 py -100
906 pz 400
c ---------------------------------------Universe-------------------------------------------------
91  SO 20000
92  SO 40000
93  SO 60000
94  SO 80000
95  SO 90000
96  SO 100000
97  SO 110000
98  SO 120000
99  SO 130000                                   $ universe sphere
```

```
c ------------------------------------DATA CARDS-------------------------------------------
-
MODE P
c  -- Source definition for asphalt only (slab is for attenuation only) –
SDEF PAR 2 CEL=6 X=D1 Y=D2 Z=D3 ERG=D15
SI1 -3700 3700
SP1 0 1
SI2 -3700 3700
SP2 0 1
SI3 -35.48 -30.48
SP3 0 1
c  -- Source definition concrete (asphalt is just an attenuator) --
c SDEF PAR 2 X=D2 Y=D5 Z=D9 ERG=D14
c SI2 -198.0 198.0       $ x for 3 cells in slab
c SP2 0 1
c SI5 -228.25 228.25     $ y for 3 cells in slab
c SP5 0 1
c SI9 -30.48 0.0         $ z for 3 cells in slab
c SP9 0 1
c -------------------------Concrete-----------------------
c  -- F1 --
SI14     L 0.09259 0.18621 0.23863 0.24200 0.29522 0.30009
         0.33832 0.35193 0.58319 0.60931 0.72733 0.91120
         0.96897 1.12029 1.23811 1.40799 1.46082 1.76449
         2.20406 2.61451
SP14     D 0.00050 0.00069 0.00312 0.02023 0.05355 0.00024
         0.00111 0.10238 0.20460 0.18382 0.00978 0.00255
         0.00156 0.06021 0.02309 0.00857 0.00323 0.06141
         0.02026 0.24011
c  -- F2 --
c SI14     L 0.09259 0.18621 0.23863 0.24200 0.29522 0.30009
c          0.33832 0.35193 0.58319 0.60931 0.72733 0.76836
c          0.91120 0.96897 1.12029 1.23811 1.40799 1.46082
c          1.76449 2.20406 2.61451
c SP14     D 0.00056 0.00070 0.00304 0.02187 0.05681 0.00023
c          0.00118 0.11067 0.20352 0.17325 0.00000 0.01857
c          0.00270 0.00165 0.05675 0.02176 0.00808 0.00288
c          0.05788 0.01909 0.23882
c  -- G1 --
c SI14     L 0.06329 0.09259 0.12907 0.18621 0.20925 0.23863
c          0.24099 0.24200 0.27024 0.27737 0.29522 0.30009
c          0.32800 0.33832 0.35193 0.40946 0.46300 0.58319
c          0.60932 0.72733 0.76836 0.78537 0.79495 0.83571
```

```
c         0.86056 0.91120 0.93406 0.96477 0.96877 1.12029
c         1.23812 1.37767 1.46082 1.72959 1.76449 2.20406
c         2.61451
c SP14     D 0.00010 0.00011 0.00025 0.00024 0.00041 0.00309
c         0.00006 0.00757 0.00036 0.02534 0.01965 0.00023
c         0.00031 0.00118 0.03829 0.00020 0.00046 0.32635
c         0.05957 0.00340 0.00638 0.00056 0.00044 0.00017
c         0.04799 0.00269 0.00392 0.00052 0.00165 0.01951
c         0.00748 0.00517 0.00312 0.00377 0.01990 0.00656
c         0.38298
c  -- G2 --
c SI14     L 0.09259 0.12907 0.18621 0.20925 0.23863 0.24099
c         0.24200 0.27024 0.27737 0.29522 0.30009 0.32800
c         0.33832 0.35193 0.40946 0.46300 0.58319 0.60932
c         0.72733 0.76836 0.79495 0.86056 0.91120 0.93406
c         0.96477 0.96877 1.12029 1.23812 1.37767 1.46082
c         1.76449 2.20406 2.61451
c SP14     D 0.00021 0.00023 0.00023 0.00037 0.00321 0.00007
c         0.00823 0.00033 0.02494 0.02137 0.00024 0.00028
c         0.00106 0.04162 0.00018 0.00041 0.32124 0.06480
c         0.00358 0.00694 0.00040 0.04724 0.00243 0.00426
c         0.00047 0.00149 0.02123 0.00814 0.00562 0.00340
c         0.02165 0.00714 0.37699
c  -- L1 --
c SI14     L 0.09259 0.18621 0.23863 0.24200 0.29522 0.33832
c         0.35193 0.58319 0.60932 0.91120 0.96877 1.12029
c         1.23812 1.46082 1.76449 2.61451
c SP14     D 0.00034 0.00050 0.00348 0.01497 0.03889 0.00113
c         0.07576 0.30633 0.10513 0.00260 0.00159 0.03444
c         0.01320 0.00703 0.03512 0.35949
c  -- L2 --
c SI14     L 0.09259 0.18621 0.23863 0.24200 0.29522 0.33832
c         0.35193 0.46300 0.58319 0.60932 0.72733 0.91120
c         0.96877 1.12029 1.46082 1.76449 2.61451
c SP14     D 0.00049 0.00068 0.00364 0.01822 0.04733 0.00119
c         0.09220 0.00046 0.28416 0.12047 0.00597 0.00272
c         0.00167 0.03946 0.00764 0.04024 0.33347
c ----------Asphalt Source----------
SI15     L 0.09259 0.18621 0.23863 0.24200 0.29522 0.30009
         0.33832 0.35193 0.58319 0.60931 0.72733 0.91120
         0.96897 1.12029 1.23811 1.40799 1.46082 1.76449
         2.20406 2.61451
SP15     D 0.00050 0.00069 0.00312 0.02023 0.05355 0.00024
         0.00111 0.10238 0.20460 0.18382 0.00978 0.00255
```

```
          0.00156 0.06021 0.02309 0.00857 0.00323 0.06141
          0.02026 0.24011
c ----------------Material Specifications----------------
c --------------------F1 Concrete-------------------------
c m1    01000 -0.033711
      06000 -0.003921  $ Carbon in Concrete
      08000 -0.531250  $ Oxygen in Concrete
      11000 -0.014077  $ Sodium in Concrete
      12000 -0.001097  $ Magnesium in Concrete
      13000 -0.017120  $ Aluminum in Concrete
      14000 -0.348819  $ Silicon in Concrete
      19000 -0.011478  $ Potassium in Concrete
      20000 -0.033314  $ Calcium in Concrete
      25000 -0.000304  $ Manganese in Concrete
      26000 -0.005214  $ Iron in Concrete
c
c --------------------F2 Concrete-------------------------
c m1    01000 -0.017612  $ Hydrogen in Concrete
c       06000 -0.001958  $ Carbon in Concrete
c       08000 -0.549496  $ Oxygen in Concrete
c       11000 -0.014511  $ Sodium in Concrete
c       12000 -0.001282  $ Magnesium in Concrete
c       13000 -0.021241  $ Aluminum in Concrete
c       14000 -0.313240  $ Silicon in Concrete
c       19000 -0.010240  $ Potassium in Concrete
c       20000 -0.061909  $ Calcium in Concrete
c       26000 -0.008511  $ Iron in Concrete
c
c --------------------G1 Concrete-------------------------
c m1    01000 -0.080161  $ Hydrogen in Concrete
c       06000 -0.009936  $ Carbon in Concrete
c       08000 -0.510624  $ Oxygen in Concrete
c       11000 -0.013599  $ Sodium in Concrete
c       12000 -0.000886  $ Magnesium in Concrete
c       13000 -0.012496  $ Aluminum in Concrete
c       14000 -0.346864  $ Silicon in Concrete
c       19000 -0.011651  $ Potassium in Concrete
c       20000 -0.011204  $ Calcium in Concrete
c       26000 -0.002580  $ Iron in Concrete
c
c --------------------G2 Concrete-------------------------
c m1    01000 -0.124999  $ Hydrogen in Concrete
c       06000 -0.016375  $ Carbon in Concrete
c       08000 -0.399632  $ Oxygen in Concrete
```

```
c       11000 -0.010649  $ Sodium in Concrete
c       12000 -0.000677  $ Magnesium in Concrete
c       13000 -0.010184  $ Aluminum in Concrete
c       14000 -0.408146  $ Silicon in Concrete
c       19000 -0.013620  $ Potassium in Concrete
c       20000 -0.013082  $ Calcium in Concrete
c       26000 -0.002638  $ Iron in Concrete
c
c --------------------L1 Concrete-------------------------
c m1    01000 -0.029552  $ Hydrogen in Concrete
c       06000 -0.003369  $ Carbon in Concrete
c       08000 -0.614243  $ Oxygen in Concrete
c       11000 -0.016252  $ Sodium in Concrete
c       12000 -0.001340  $ Magnesium in Concrete
c       13000 -0.021627  $ Aluminum in Concrete
c       14000 -0.245125  $ Silicon in Concrete
c       19000 -0.008155  $ Potassium in Concrete
c       20000 -0.052694  $ Calcium in Concrete
c       26000 -0.007642  $ Iron in Concrete
c
c --------------------L2 Concrete-------------------------
c m1    01000 -0.119111  $ Hydrogen in Concrete
c       06000 -0.016020  $ Carbon in Concrete
c       08000 -0.283515  $ Oxygen in Concrete
c       11000 -0.007545  $ Sodium in Concrete
c       12000 -0.000492  $ Magnesium in Concrete
c       13000 -0.008039  $ Aluminum in Concrete
c       14000 -0.528034  $ Silicon in Concrete
c       19000 -0.017544  $ Potassium in Concrete
c       20000 -0.016893  $ Calcium in Concrete
c       26000 -0.002808  $ Iron in Concrete
c
c ---------------Aluminum, Structural 6061-----------------
m2    13000 -0.9685    $ Aluminum
      26000 -0.0070    $ Iron
      29000 -0.0025    $ Copper
      14000 -0.0060    $ Silicon
      12000 -0.0110    $ Magnesium
      24000 -0.0035    $ Chromium
      25000 -0.0015    $ Manganese
c ------------Air (suitable for breathing!)----------------
m3    06000 -0.000124  $ Carbon in Air
      07000 -0.755268  $ Nitrogen in Air
      08000 -0.231781  $ Oxygen in Air
```

```
     18000 -0.012827  $ Argon in Air
c ----------------PVT Scintillator----------------------
m4    01000 -0.085000   $ Hydrogen in PVT
      06000 -0.915000   $ Carbon in PVT
c ---------------Steel, Stainless 304---------------------
m5    24000 -0.190000   $ Chromium in Steel
      25000 -0.020000   $ Manganese in Steel
      26000 -0.695000   $ Iron in Steel
      28000 -0.095000   $ Nickel in Steel
c --------------------Lead-------------------------------
m6    82000 -1.000000   $ Pure lead
c ------------PMMA (Light Pipe Lucite)--------------------
m7    01000 -0.080538   $ Hydrogen in PMMA
      06000 -0.599848   $ Carbon in PMMA
      08000 -0.319614   $ Oxygen in PMMA
c -----------------Carbon Steel---------------------------
m8   06000 -0.005      $ Carbon in Steel
    26000 -0.995      $ Iron in Steel
c ------------------Asphalt-------------------------------
m9    1000 -0.016403
      6000  -0.351452
      7000  -0.000260
      8000  -0.329185
     11000  -0.008377
     12000  -0.016291
     13000  -0.032877
     14000  -0.145583
     16000  -0.001787
     19000  -0.011626
     20000  -0.061911
     22000  -0.002479
     23000  -0.000015
     25000  -0.000223
     26000  -0.020229
     28000  -0.000001
     82000  -0.001303
M10   14028  0.333343  8016  0.666657              $ SiO2
m11   1001  -0.1437    6012 -0.8563               $ Polyethylene
m12   6012   -0.0008  25055 -0.02    24052  -0.18    $ Stainless steel
      28058  -0.08    26056 -0.7085  14028  -0.01
      16032  -0.0003  15031 -0.00045
m13    2003  -1                                  $ He-3
c ----------------------------Tallies--------------------------------
c F1:P 91 92 93 94 95 96 97 98 99
```

```
c E1 0.0 0.00001 0.025 0.140 0.5 0.75 1.0 1.5 2.0 2.5 3.0  $ Energy bins
c C1 -0.866 -0.5 0 0.5 0.866 1
c F11:P 91 92 93 94 95 96 97 98 99
c E11 0.0 0.00001 0.025 0.140 0.5 0.75 1.0 1.5 2.0 2.5 3.0  $ Energy bins
c C11 -0.866 -0.5 0 0.5 0.866 1
c FT11 FRV 0 0 -1
F18:P 11                $ Pulse height tally in RIGHT LOWER detector
E18 0.0 0.00001 0.025 0.140 1.0 3.0  $ Energy bins
F28:P 12                $ Pulse height tally in RIGHT UPPER detector
E28 0.0 0.00001 0.025 0.140 1.0 3.0  $ Energy bins
F38:P 21                $ Pulse height tally in LEFT LOWER detector
E38 0.0 0.00001 0.025 0.140 1.0 3.0  $ Energy bins
F48:P 22                $ Pulse height tally in LEFT UPPER detector
E48 0.0 0.00001 0.025 0.140 1.0 3.0  $ Energy bins
NPS 1.00E8
PRDMP -60 -60
```

APPENDIX D

MCNP input deck for material transmission comparison

```
c Concrete Attenuation Experiment
c F1 concrete sample
c Cd-109 source
c
c ** Cell Cards **
c
1    1  -2.301     -1  2 -3           imp:p=1 $ concrete disk
2    2  -1.205E-3  -4  5 -6           imp:p=1 $ air filled dummy detector
3    2  -1.205E-3  -100 #1 #2         imp:p=1 $ air
4    0              100               imp:p=0 $ universe

c ** Surface Cards **
c
c     -- concrete disk surfaces --
1     cx   2.95275                    $ radius ofconcrete disk
2     px   1.143                      $ top/front of disk
3     px   3.52425                    $ bottom/back of disk
4     cx   5.08                       $ radius of "detector face"
5     px   4.03225                    $ location of "detector face"
6     px   9                          $ back of dummy detector
c
c     -- universe --
100   so   100

c ** Data Cards **
MODE P
SDEF  POS 0 0 0  ERG=0.088
c SDEF  POS 0 0 0  ERG=0.6617
c SDEF  POS 0 0 0  ERG= 1.3325
NPS   100000
c     -- Concrete --
c     -- Densitometry –
c     -- F1 –
m1    01000 -0.033711  $ Hydrogen in Concrete
      06000 -0.003921  $ Carbon in Concrete
      08000 -0.531250  $ Oxygen in Concrete
      11000 -0.014077  $ Sodium in Concrete
      12000 -0.001097  $ Magnesium in Concrete
```

```
      13000 -0.017120  $ Aluminum in Concrete
      14000 -0.348819  $ Silicon in Concrete
      19000 -0.011478  $ Potassium in Concrete
      20000 -0.033314  $ Calcium in Concrete
      25000 -0.000304  $ Manganese in Concrete
      26000 -0.005214  $ Iron in Concrete
c
c     -- F2 --
c m1    01000 -0.017612  $ Hydrogen in Concrete
c       06000 -0.001958  $ Carbon in Concrete
c       08000 -0.549496  $ Oxygen in Concrete
c       11000 -0.014511  $ Sodium in Concrete
c       12000 -0.001282  $ Magnesium in Concrete
c       13000 -0.021241  $ Aluminum in Concrete
c       14000 -0.313240  $ Silicon in Concrete
c       19000 -0.010240  $ Potassium in Concrete
c       20000 -0.061909  $ Calcium in Concrete
c       26000 -0.008511  $ Iron in Concrete
c
c     -- G1 --
c m1    01000 -0.080161  $ Hydrogen in Concrete
c       06000 -0.009936  $ Carbon in Concrete
c       08000 -0.510624  $ Oxygen in Concrete
c       11000 -0.013599  $ Sodium in Concrete
c       12000 -0.000886  $ Magnesium in Concrete
c       13000 -0.012496  $ Aluminum in Concrete
c       14000 -0.346864  $ Silicon in Concrete
c       19000 -0.011651  $ Potassium in Concrete
c       20000 -0.011204  $ Calcium in Concrete
c       26000 -0.002580  $ Iron in Concrete
c
c     -- G2 --
c m1    01000 -0.124999  $ Hydrogen in Concrete
c       06000 -0.016375  $ Carbon in Concrete
c       08000 -0.399632  $ Oxygen in Concrete
c       11000 -0.010649  $ Sodium in Concrete
c       12000 -0.000677  $ Magnesium in Concrete
c       13000 -0.010184  $ Aluminum in Concrete
c       14000 -0.408146  $ Silicon in Concrete
c       19000 -0.013620  $ Potassium in Concrete
c       20000 -0.013082  $ Calcium in Concrete
c       26000 -0.002638  $ Iron in Concrete
c
c     -- L1 –
```

```
c m1    01000 -0.029552  $ Hydrogen in Concrete
c       06000 -0.003369  $ Carbon in Concrete
c       08000 -0.614243  $ Oxygen in Concrete
c       11000 -0.016252  $ Sodium in Concrete
c       12000 -0.001340  $ Magnesium in Concrete
c       13000 -0.021627  $ Aluminum in Concrete
c       14000 -0.245125  $ Silicon in Concrete
c       19000 -0.008155  $ Potassium in Concrete
c       20000 -0.052694  $ Calcium in Concrete
c       26000 -0.007642  $ Iron in Concrete
c
c     -- L2 –
c m1    01000 -0.119111  $ Hydrogen in Concrete
c       06000 -0.016020  $ Carbon in Concrete
c       08000 -0.283515  $ Oxygen in Concrete
c       11000 -0.007545  $ Sodium in Concrete
c       12000 -0.000492  $ Magnesium in Concrete
c       13000 -0.008039  $ Aluminum in Concrete
c       14000 -0.528034  $ Silicon in Concrete
c       19000 -0.017544  $ Potassium in Concrete
c       20000 -0.016893  $ Calcium in Concrete
c       26000 -0.002808  $ Iron in Concrete
c
c     -- NAA--
c     -- F1 --
c m1    01000 -0.005000  $ Hydrogen in Concrete
c       06000 -0.162900  $ Carbon in Concrete
c       08000 -0.484500  $ Oxygen in Concrete
c       11000 -0.000260  $ Sodium in Concrete
c       12000 -0.011900  $ Magnesium in Concrete
c       13000 -0.004440  $ Aluminum in Concrete
c       14000 -0.015100  $ Silicon in Concrete
c       19000 -0.001087  $ Potassium in Concrete
c       20000 -0.310100  $ Calcium in Concrete
c       25000 -0.000304  $ Manganese in Concrete
c       26000 -0.004366  $ Iron in Concrete
c     -- F2 --
c m1    01000 -0.005000  $ Hydrogen in Concrete
c       06000 -0.146100  $ Carbon in Concrete
c       08000 -0.487200  $ Oxygen in Concrete
c       11000 -0.000324  $ Sodium in Concrete
c       12000 -0.010600  $ Magnesium in Concrete
c       13000 -0.006236  $ Aluminum in Concrete
c       14000 -0.018600  $ Silicon in Concrete
```

```
c      19000 -0.001683  $ Potassium in Concrete
c      20000 -0.318800  $ Calcium in Concrete
c      25000 -0.000355  $ Manganese in Concrete
c      26000 -0.005406  $ Iron in Concrete
c     -- G1 --
c m1    01000 -0.005000  $ Hydrogen in Concrete
c      06000 -0.023300  $ Carbon in Concrete
c      08000 -0.472700  $ Oxygen in Concrete
c      11000 -0.018700  $ Sodium in Concrete
c      12000 -0.003781  $ Magnesium in Concrete
c      13000 -0.061800  $ Aluminum in Concrete
c      14000 -0.266200  $ Silicon in Concrete
c      19000 -0.026600  $ Potassium in Concrete
c      20000 -0.100600  $ Calcium in Concrete
c      25000 -0.000785  $ Manganese in Concrete
c      26000 -0.021300  $ Iron in Concrete
c    -- G2 --
c m1    06000 -0.000500  $ Carbon in Concrete
c      08000 -0.473100  $ Oxygen in Concrete
c      11000 -0.020000  $ Sodium in Concrete
c      12000 -0.003594  $ Magnesium in Concrete
c      13000 -0.066000  $ Aluminum in Concrete
c      14000 -0.295200  $ Silicon in Concrete
c      19000 -0.032700  $ Potassium in Concrete
c      20000 -0.089800  $ Calcium in Concrete
c      25000 -0.001153  $ Manganese in Concrete
c      26000 -0.019100  $ Iron in Concrete
c     -- L1 --
c m1    01000 -0.005000  $ Hydrogen in Concrete
c      06000 -0.142900  $ Carbon in Concrete
c      08000 -0.476900  $ Oxygen in Concrete
c      11000 -0.000732  $ Sodium in Concrete
c      12000 -0.010900  $ Magnesium in Concrete
c      13000 -0.015300  $ Aluminum in Concrete
c      14000 -0.047500  $ Silicon in Concrete
c      19000 -0.006900  $ Potassium in Concrete
c      20000 -0.284800  $ Calcium in Concrete
c      25000 -0.000482  $ Manganese in Concrete
c      26000 -0.009090  $ Iron in Concrete
c     -- L2 --
c m1    01000 -0.005000  $ Hydrogen in Concrete
c      06000 -0.119400  $ Carbon in Concrete
c      08000 -0.482100  $ Oxygen in Concrete
c      11000 -0.001022  $ Sodium in Concrete
```

```
c       12000 -0.008900  $ Magnesium in Concrete
c       13000 -0.017400  $ Aluminum in Concrete
c       14000 -0.053300  $ Silicon in Concrete
c       19000 -0.007705  $ Potassium in Concrete
c       20000 -0.294600  $ Calcium in Concrete
c       25000 -0.000501  $ Manganese in Concrete
c       26000 -0.001507  $ Iron in Concrete
c
c     -- Air --
m2    06000 -0.000124  $ Carbon in Air
      07000 -0.755268  $ Nitrogen in Air
      08000 -0.231781  $ Oxygen in Air
      18000 -0.012827  $ Argon in Air
c     -- Tally --
F1:P  5               $ current across surface 5
E1    0.0865 0.0891    $ energy bin
c E1    0.6587 0.6638    $ energy bin
c E1    1.3293 1.3355    $ energy bin
```